Chaos

Random dynamics of the Morris–Lecar neural model

Cite as: Chaos **14**, 511 (2004); https://doi.org/10.1063/1.1756118
Submitted: 25 November 2003 . Accepted: 08 April 2004 . Published Online: 10 June 2004

Takashi Tateno, and Khashayar Pakdaman

REGULAR ARTICLES

Random dynamics of the Morris–Lecar neural model

Takashi Tateno[a)]
Department of Physiology, University of Cambridge, Downing Street, Cambridge CB2 3EG, United Kingdom

Khashayar Pakdaman[b)]
Inserm U444 Faculté de Médecine Saint-Antoine 27, rue Chaligny 75571, Paris Cedex 12, France

(Received 25 November 2003; accepted 8 April 2004; published online 10 June 2004)

Determining the response characteristics of neurons to fluctuating noise-like inputs similar to realistic stimuli is essential for understanding neuronal coding. This study addresses this issue by providing a random dynamical system analysis of the Morris–Lecar neural model driven by a white Gaussian noise current. Depending on parameter selections, the deterministic Morris–Lecar model can be considered as a canonical prototype for widely encountered classes of neuronal membranes, referred to as class I and class II membranes. In both the transitions from excitable to oscillating regimes are associated with different bifurcation scenarios. This work examines how random perturbations affect these two bifurcation scenarios. It is first numerically shown that the Morris–Lecar model driven by white Gaussian noise current tends to have a unique stationary distribution in the phase space. Numerical evaluations also reveal quantitative and qualitative changes in this distribution in the vicinity of the bifurcations of the deterministic system. However, these changes notwithstanding, our numerical simulations show that the Lyapunov exponents of the system remain negative in these parameter regions, indicating that no dynamical stochastic bifurcations take place. Moreover, our numerical simulations confirm that, regardless of the asymptotic dynamics of the deterministic system, the random Morris–Lecar model stabilizes at a unique stationary stochastic process. In terms of random dynamical system theory, our analysis shows that additive noise destroys the above-mentioned bifurcation sequences that characterize class I and class II regimes in the Morris–Lecar model. The interpretation of this result in terms of neuronal coding is that, despite the differences in the deterministic dynamics of class I and class II membranes, their responses to noise-like stimuli present a reliable feature.
[DOI: 10.1063/1.1756118]

A fundamental issue for understanding information coding in nervous systems is that of neuronal reliability. As pointed out by Movshon,[1] neural responses to an identical stimulus *in vivo* are unreliable from moment to moment. Identical stimuli delivered to neurons never elicit precise responses on repeated trials. Recently, neural variability and its importance for the signal processing have been most intensively investigated in experimental and computational neuroscience studies. However, little has been performed from the theoretical and analytical points of view. From the standpoint of random dynamical system theory, we tackled this issue for a simple but realistic neural model, the Morris–Lecar (ML) equations. Qualitative difference of response characteristics in the ML model generates two bifurcation scenarios. We found that additive stochastic perturbations completely destroy the bifurcation scenarios. In other words, noise-like stimulus does not induce any stochastic dynamical bifurcations. Moreover, we found that the ML model evoked by noise-like stimulus has an asymptotically stable stochastic attractor. This implies that if the ML model is initiated at a different state point and presented with the same noise-like input repeatedly, the same response will be evoked after a transient time. In this sense, the ML-model response evoked by such noise-like input is reliable. These results should help to elucidate neural coding in actual neural systems.

I. INTRODUCTION

Neurons respond to stimuli by generating sequences of brief electrical pulses, referred to as action potentials. The form of action potentials varies little, so that information concerning the stimulus cannot be readily conveyed by their shape. Conversely, the timing of these electrical discharges is stimulus dependent, so that elucidating the neuronal code consists essentially in determining the relation between some stimulation and the discharge train it evokes. This study ad-

[a)]Electronic mail: tt259@cam.ac.uk
[b)]Present address: Institut Jacques Monod, CNRS, Universites Paris 6, Paris 7, 2 Place Jussieu, 75251 Paris Cedex 05, France.

dresses this issue by analyzing the response of a canonical membrane model, namely the Morris–Lecar (ML) model,[2] to white Gaussian noise current stimulation considered as a realistic model for the inputs of some neurons *in vivo*.

The response of neurons to periodic stimuli such as sinusoidal currents, as well as periodic pulse trains have been widely studied.[3–6] These have revealed that such stimuli evoke diverse firing patterns that are phase locked, quasiperiodic or chaotic. A large number of theoretical analyses have been devoted to characterize these behaviors from the standpoint of the geometrical theory of dynamical systems and determine the conditions for their occurrence through systematic bifurcation analysis (e.g., Refs. 7, 8, and references therein).

In this study, we are concerned with the response of neurons to a different form of stimulation, namely a white Gaussian noise current. Gaussian current stimulation has been used in *in vitro* experiments that attempt to reproduce the response of neurons to realistic stimulus. Indeed the inputs some neurons in central nervous system, such as neocortical cells, receive can be well approximated by highly fluctuating aperiodic signals such as the sample path of a Gaussian process.[9]

In a seminal study, Bryant and Segundo[10] observed that such stimuli evoke reliable discharge times, in the sense that when the neuron is stimulated repeatedly with the same Gaussian sample path, there is little variability in the timing of action potentials from one trial to another. Bryant and Segundo performed their experiment using well identified neurons of the sea slug aplysia. Since then, their observation has been consistently reproduced in a wide variety of preparations such as rat muscle spindles subject to Gaussian mechanical stimuli,[11] rat neocortical neurons,[9] aplysia buccal pacemaker cells,[12] and various stages of the visual system of insects and vertebrates subject to aperiodically fluctuating light stimuli.[13–15]

In this study, we perform a numerical analysis of neuronal behavior in response to white Gaussian noise current. As mentioned above, the geometrical methods of dynamical system theory have been highly successful in elucidating the response of neurons to periodic stimuli. Here, we use a different approach, based on random dynamical system (RDS) theory.[16] The random dynamics of systems forced by Gaussian noise can considerably differ from their deterministic counterpart. Highly illustrative examples of such differences are the destruction of various bifurcations, such as pitchfork bifurcation in scalar systems[17] and Hopf bifurcation in the stochastic Brusselator by additive white Gaussian noise,[18] or, the onset of stochastic chaos in the noisy Kramer's oscillator.[19]

Previous studies of random dynamical systems applied to neuronal models have also revealed that the response of neuronal models to white Gaussian noise can take on diverse forms, with for instance the active rotator[20] and the Hodgkin–Huxley model being exempt of dynamic stochastic bifurcations,[21] while, in contrast, the FitzHugh–Nagumo can switch to a regime of stochastic chaos.[22,23]

This work is concerned with the random dynamics of the ML model. This model which was first introduced to account for electrical activity of the barnacle muscle fibers has, since then, become a canonical neuronal model because for different parameter regimes, it displays two important forms of neuronal behavior. From the standpoint of the geometrical theory of dynamical systems, these forms correspond to two different bifurcation scenarios between a stable equilibrium point and a stable limit cycle. In the first one, the limit cycle appears through a saddle-node separatrix-loop bifurcation, while in the second one it is through a double limit cycle bifurcation followed by a subcritical Hopf bifurcation. The main purpose of this work is to analyze the influence of random perturbations upon these two scenarios. In fact, our study suggests that additive noise destroys both bifurcation sequences in the sense of the stochastic bifurcation theory. However, we also show that the characteristics of the stationary stochastic process associated with the stochastic ML model depend both on the noise intensity and the behavior of the deterministic system.

This paper is organized as follows: In Sec. II, we introduce the deterministic ML model and review the two types of behavior it displays. In Sec. III, the stochastic ML model is described. In Sec. IV, the stochastic approach is explained and its numerical results are presented. In Sec. V, the RDS approach is addressed. In Sec. VI, numerical results on the RDS approach are provided. In Sec. VII, we finally discuss our results.

II. THE DETERMINISTIC MORRIS–LECAR MODEL

This section presents first the ML model, and then reviews the dynamics of this model for two different parameter sets that reproduce the behavior of class I and class II neuronal membranes. These were first described by Rinzel and Ermentrout,[24] and our presentation closely follows theirs.

A. The Morris–Lecar model

The ML model is a mathematical model for the barnacle muscle fiber.[2] The ML model belongs to the vast family of conductance-based membrane models of which Hodgkin–Huxley (HH) model is a well-known archetype.[25] The ML equations represent an electrical circuit equivalent to a cellular membrane crossed by three different transmembranar currents, referred to, respectively, as the voltage-gated Ca^{2+} current, the voltage-gated delayed-rectifier K^+ current and the leak current.[2] Figure 1 shows the equivalent circuit hypothesized for a space-clamped patch of sarcolemma membrane of the barnacle muscle fiber.

The original ML model is a third-order nonlinear system of a Hodgkin–Huxley form whose variables represent the voltage and Ca^{2+} and K^+ activations. Taking advantage of the fact that the second variable is much faster than the third one, Morris and Lecar reduced the original model to a two-dimensional system by assuming that Ca^{2+} activation reaches instantaneously its steady state value.[2] Our study is concerned with this reduced version of the model which is widely referred to as the ML model in the literature. The ML model is represented by the following second-order system:

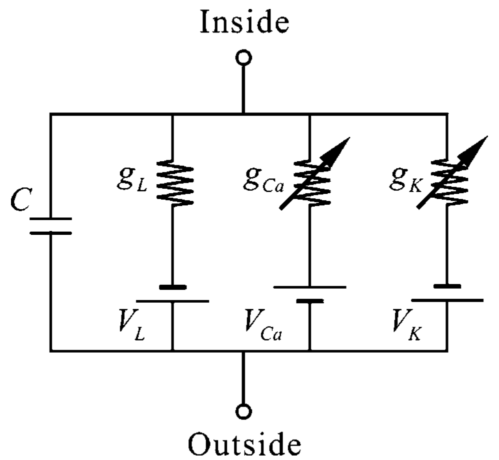

FIG. 1. Equivalent circuit for a patch of space-clamped barnacle sarcolemma. The membrane current can divide into four pathways: one is capacitative, and three are conductive pathways in series with the associated reversal potentials, shown as batteries.

$$C\frac{dv_t}{dt}=-g_{\mathrm{Ca}}m_\infty(v_t)(v_t-V_{\mathrm{Ca}})-g_{\mathrm{K}}w_t\cdot(v_t-V_{\mathrm{K}})$$
$$-g_{\mathrm{L}}(v_t-V_{\mathrm{L}})+I, \tag{1a}$$

$$\frac{dw_t}{dt}=\phi\frac{w_\infty(v_t)-w_t}{\tau_w(v_t)}, \tag{1b}$$

where

$$m_\infty(v)=0.5\left[1+\tanh\left(\frac{v-V_1}{V_2}\right)\right], \tag{2a}$$

$$w_\infty(v)=0.5\left[1+\tanh\left(\frac{v-V_3}{V_4}\right)\right], \tag{2b}$$

$$\tau_w(v)=\left[\cosh\left(\frac{v-V_3}{2V_4}\right)\right]^{-1}. \tag{2c}$$

The three terms in the right-hand side of Eq. (1a) represent successively the voltage-gated Ca^{2+} current, the voltage-gated delayed-rectifier K^+ current, and the leak current. In Eq. (1), the variables v_t and w_t represent the membrane voltage and the activation of delayed rectifier K^+ current. The parameters g_{Ca}, g_{K}, and g_{L} are the maximal conductances associated with the three transmembranar currents, and, V_{Ca}, V_{K}, and V_{L} are the corresponding reversal potentials. Input current is represented by I. Finally the constant ϕ in Eq. (1b) determines the scaling of the rate for K^+ channel opening.

The two parameter sets used throughout this study are the same as those described by Rinzel and Ermentrout.[24] Their values are listed in the Appendix. The rational for selecting these two parameter sets is explained in the following section, which also describes the dynamics of the deterministic ML model for these parameter values.

B. Class I and class II membranes

Here, we briefly explain the class I and II excitability we referred to in this paper. Neuronal membranes generate brief electrical pulses referred to as action potentials or spikes. Roughly speaking, a membrane may be excitable or oscillating. In the former, the membrane potential stabilizes at a resting state, while in the latter, it undergoes periodic oscillations due to periodic generation of action potentials. An excitable membrane may also generate action potential if stimulated by a strong enough input such as a sufficiently large current pulse. In such a situation, the time interval separating the onset of the stimulus from the onset of the action potential is referred to as the spike latency. It represents the delay between the stimulation and the membrane response.

Excitable membranes may be transformed into oscillating ones and vice versa by changing experimental conditions. For instance, in some experimental preparations, an excitable membrane, that is one that stabilizes at a constant resting potential, may be rendered oscillating, that is forced to periodically generate action potentials, through the injection of a well-adjusted constant direct current.

The separation of membranes into class I and class II is based upon phenomenological descriptions of excitable and oscillating regimes, and the transition between the two. In a systematic study of the response of isolated axons of *Carcinus maenas* to various amplitudes of rectangular current stimuli, Hodgkin found that some oscillating axons could be made to fire with arbitrarily low response frequencies, while others could not.[26] The discharge frequencies of the latter class of axons lie within a narrow range and were clearly distinct from zero. Furthermore, the first axons could display considerable spike latencies, while in the second ones, the time delay between stimulation and response was not substantial. Hodgkin referred to the first type of membrane as class I and to the second type as class II. Hodgkin's results are in general agreement with those obtained in other preparations, such as *Cancer pagurus* axons[27] and decalcified nerves of frogs and squids.[28] For this reason, Hodgkin's classification is considered to be representative of the behavior of a wide variety of neurons.

In the same way as experimental preparations, Hodgkin–Huxley-type single-neuron models commonly used in theoretical neurosciences are also classified into class I or class II categories. Rinzel and Ermentrout proposed an interpretation of these membrane classes in terms of the phase portraits and bifurcation diagrams of the mathematical models.[24] Since they carried their analysis using the ML model, this model has become the canonical system in which the characteristics of each class of membrane is investigated. For the sake of self-containment, we briefly present an analysis of the ML model in class I and class II regimes, and describe the corresponding bifurcation diagrams.

1. Class I

Figure 2(A) is the bifurcation diagram of the ML model with the class I parameter set. The lines in Fig. 2(A) represent the steady-state voltage v versus I and the maximum and minimum voltage for periodic solutions. For $I<I_c \simeq 40\ \mu\mathrm{A/cm}^2$, there are three equilibrium points, the lower one being a stable node, the middle one a saddle point and the upper one an unstable focus. For $I>I_c$, only the unstable point subsists surrounded by a stable limit cycle. At $I=I_c$,

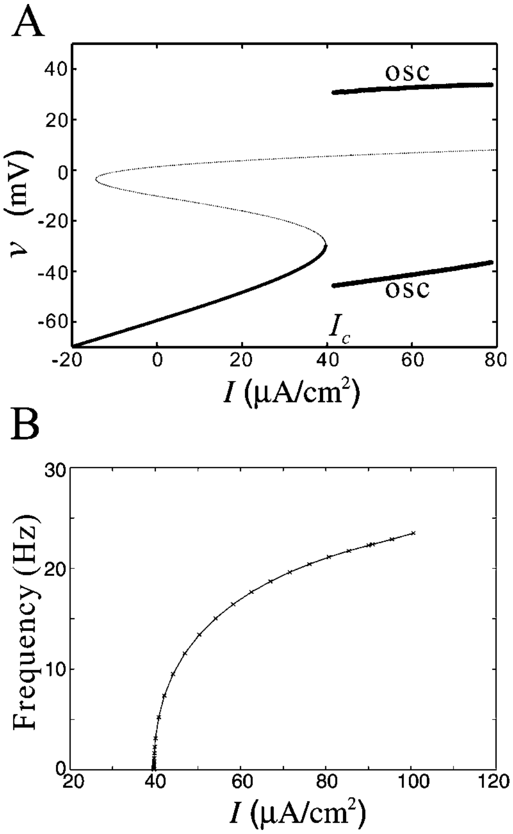

FIG. 2. (A) Bifurcation diagram of the class I ML model. The thick curves stand for stable solutions and the thin curve for unstable ones. Repetitive firing occurs for the critical current $I_c \simeq 40$ μA/cm^2, where the stable rest state and saddle coalesce. Branches labeled ''osc'' respectively represent maximum and minimum values of v in each periodic solution. Abscissa: stimulus current intensity I (μA/cm^2), ordinate: membrane voltage v (mV). (B) Frequency of stable periodic solutions versus I. With increasing the current intensity, the frequency is monotonically increasing from zero frequency at the critical current.

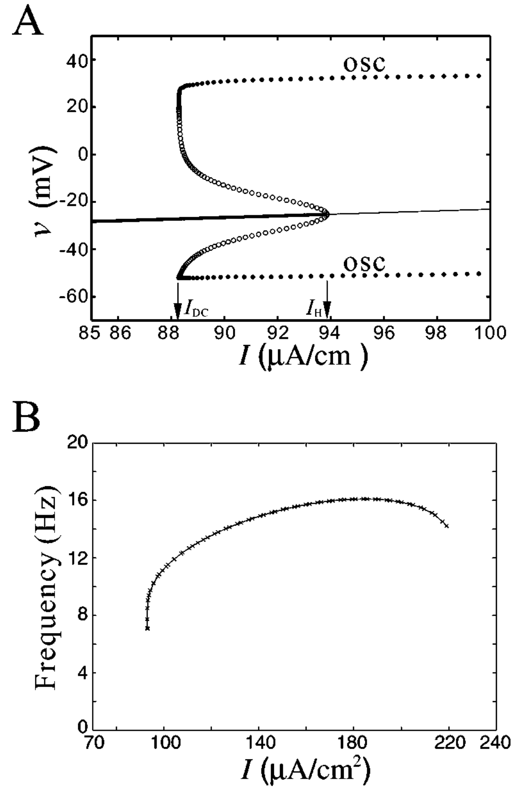

FIG. 3. (A) Bifurcation diagram of the class II ML model. The system possesses a unique equilibrium point for all values of I in the parameter region shown here. The thick curve stands for stable equilibrium points for $I < I_H \simeq 93.86$ (μA/cm^2) and the thin curve for unstable ones. Amplitude of stable periodic solutions (labeled ''osc'') is indicated by maximum and minimum values of v over one period for $I > I_{DC} \simeq 88.29$ (μA/cm^2). Stability of the periodic solutions is also shown as filled (stable) and unfilled (unstable) circles. Abscissa: stimulus current intensity I (μA/cm^2), ordinate: membrane voltage v (mV). (B) Frequency of stable periodic solutions versus I. Frequency is monotone over the I parameter range of periodic solutions and the minimum firing frequency has a nonzero value.

the stable node, the saddle point and the limit cycle collide and form a saddle-node loop, also referred to as a saddle-node on an invariant circle.

The bifurcation scenario depicted above indicates that the transition to repetitive firing is marked by arbitrarily low frequency. That is, a class I membrane is observationally recognized by a continuous response frequency to an input current (FI) curve that shows oscillations arising with arbitrarily low frequencies as shown in Fig. 2(B). This limit cycle is approximately of constant amplitude, but the period depends on the amplitude of the input current I. The FI curve thus shows that the class I cell can produce a wide range of firing frequencies and that the limit cycle has an infinite period when $I = I_c$.

In the excitable regime, the stable manifold of the saddle point acts as the firing threshold. Depending on their strength, impulsive perturbations of the stable equilibrium can take the system on either side of this manifold. Those that are in the same side as the stable equilibrium produce subthreshold responses. The others evoke a discharge, that is, the system returns to the stable equilibrium point along the longer heteroclinic connection between the saddle and the stable equilibrium. There is a critical perturbation that would take the system exactly on the stable manifold of the saddle. This is called the threshold perturbation: For this exact value, the system does not return to the stable equilibrium, instead it converges to the saddle point. The closer the perturbation amplitude is to this value and the longer it takes for the system to return to the equilibrium point. This phenomenon accounts for the long spike latency times, and their dependence on perturbation amplitude.

2. Class II

The bifurcation scheme of the ML model with class II parameter set substantially differs from the one depicted above [Fig. 3(A)]. In this case the system possesses a unique equilibrium point for all values of I. This equilibrium is stable for $I \leqslant I_H \simeq 93.86$ μA/cm^2, and unstable beyond this point. The loss of stability occurs through a subcritical Hopf bifurcation. The branch of unstable periodic solutions appearing from this bifurcation expand to lower values of I, until $I_{DC} \simeq 88.29$ μA/cm^2 where they collide, at a double cycle bifurcation, with a branch a stable periodic solutions. The latter branch exists for $I > I_{DC}$ and until 216.9 μA/cm^2. The diagram shows that the system stabilizes at a unique equilibrium point for $I < I_{DC}$, while trajectories of all initial conditions except the unstable equilibrium stabilize at the limit cycle for $I \geqslant I_H$. Between these two values, i.e., $I_{DC} \leqslant I \leqslant I_H$, the stable equilibrium and limit cycle coexist and the unstable limit cycle separates their respective attraction basins. The bifurcation scenario of the class II ML model accounts for the discontinuous FI curves with the oscillations arising with a nonzero frequency. The response frequency range is narrow and largely independent of the current I as plotted in Fig. 3(B).

The excitable regimes of the class I and II ML models also differ in that in the latter there is no true threshold for the appearance of spikes. In this case, the response of the ML model is not an all-or-nothing phenomenon. When a pulse stimulus evokes a spike, the amplitude of the spike can depend on the size of the pulse stimulus. The delay to a spike is less sensitive to the size of the suprathreshold stimulus than in the class I membrane, and spike latency times remain bounded.

III. THE STOCHASTIC MORRIS–LECAR MODEL

Our purpose in this work is to analyze the influence of fluctuating noise-like perturbations on class I and class II regimes of the ML model. Such perturbations are represented by a white Gaussian noise current added to the membrane voltage. The dynamics of the ML model subjected to such a stimulation is described by the following stochastic differential equations (SDEs):

$$C dv_t = [-g_{\mathrm{Ca}} m_\infty(v_t)(v_t - V_{\mathrm{Ca}}) - g_{\mathrm{K}} w_t \cdot (v_t - V_{\mathrm{K}}) - g_L(v_t - V_L) + I] dt + \sigma dW_t, \tag{3a}$$

$$dw_t = \phi \frac{w_\infty(v_t) - w_t}{\tau_w(v_t)} dt, \tag{3b}$$

where I is an external current and σ is a noise intensity. Here, W_t represents the standard Wiener process. More precisely, let Ω be the space of continuous functions $\omega:\mathbb{R}\to\mathbb{R}$, $\mathcal{F}$ the Borel σ-algebra of subsets of Ω, and $\mathbb{P}$ the Wiener measure (distribution of W) on $\mathcal{F}$. Thus, the triplet $(\Omega, \mathcal{F}, \mathbb{P})$ is called a probability space as usual. We denote a given sample path of the process by W_t for each ω and write $W_t = \{W_t(\omega)\}$ $(0 \leqslant t < \infty)$.

The analysis of dynamical systems perturbed by noise can be carried out from different standpoints. Here, we describe two of them. To avoid ambiguity, we refer to the first as the stochastic description and to the second as the RDS theory. Given the novelty of the RDS theory and the fact that there are only few studies of neuronal models from this standpoint, we provide in the following section a heuristic description of the two stochastic and RDS approaches to clarify the differences between them. Then, we present their applications to the ML model. Comprehensive treatments of the stochastic and RDS theories are given by Lasota and Mackey[29] and Arnold.[16]

IV. THE STOCHASTIC APPROACH

In smooth deterministic systems, the initial condition uniquely determines the state of the system at any future time. In systems perturbed by noise, the state of the system at a future time depends not only on the initial condition, but also on the noise realization impinging upon the system. Different noise realizations lead to different states. Noise realizations occur with a certain probability. This probability determines the probability of reaching a certain region of the phase space at a given time starting from an initial condition. For instance, let X_0 and $X=(x_1,\ldots,x_n)$ be two points in the state space. Starting at X_0, there is a certain transition probability, denoted by $P(t,X,X_0)dx_1 dx_2 \ldots dx_n$, to reach a small neighborhood of X at time t. The stochastic approach, rather than examining the evolution of the initial condition X_0 under the influence of a single noise sample path, studies the changes of the distribution P of solutions starting at X_0. Notably the stochastic approach determines whether the probability density function (pdf) $P(t,X,X_0)$ stabilizes in the long run as $t\to+\infty$ at a uniquely determined function $\rho(X)$ independently from the initial state X_0. We refer to such a function ρ, when it exists, as the stationary distribution of the system. The shape of ρ depends on system parameters and noise intensity. The shapes of ρ at different parameter values or different noise intensities may be qualitatively different. The changes from one shape to another are referred to as phenomenological stochastic bifurcations, shortened as P-bifurcations.[16] Characterizing P-bifurcations is one method to detect changes in the behavior of noisy systems. In the remainder of this section, we examine whether such bifurcations occur in the ML model in the class I and class II regimes.

Prior to the determination of P-bifurcations, we need to discuss the existence and the uniqueness of the stationary distribution ρ for the stochastic ML model. While to our knowledge there are no rigorous proofs of this fact, a number of formal arguments similar to those presented in Ref. 18, together with extensive numerical explorations suggest that it is so. Therefore, henceforth, we assume that all transition pdfs of the stochastic ML model, whether in class I or class II regimes, stabilize at a unique stationary distribution ρ.

Determining whether the stochastic ML presents P-bifurcations or not is based upon the numerical estimation of the stationary distribution ρ. Practically, estimates of ρ for different parameter sets were obtained from numerical simulations as described in the Appendix. We continued the calculation for a sufficiently long time and observed that there was no clear change of the shape of the densities until the last time except for a first transient period.

A. The stationary distribution in the class I regime

There are essentially two types of deterministic dynamics in the class I regime. Either, the system is excitable or it is oscillating. For each type of dynamics, we describe how the shape of the stationary distribution ρ changes with the noise intensity.

When the ML model is excitable, ρ takes on a shape close to a Gaussian distribution centered on the stable equilibrium point at low noise intensities (panel A1 in Fig. 4). This indicates that the influence of weak perturbations is mainly to induce small perturbations in the vicinity of the stable equilibrium point. However, this does not preclude occasional large noise induced excursions that take the sys-

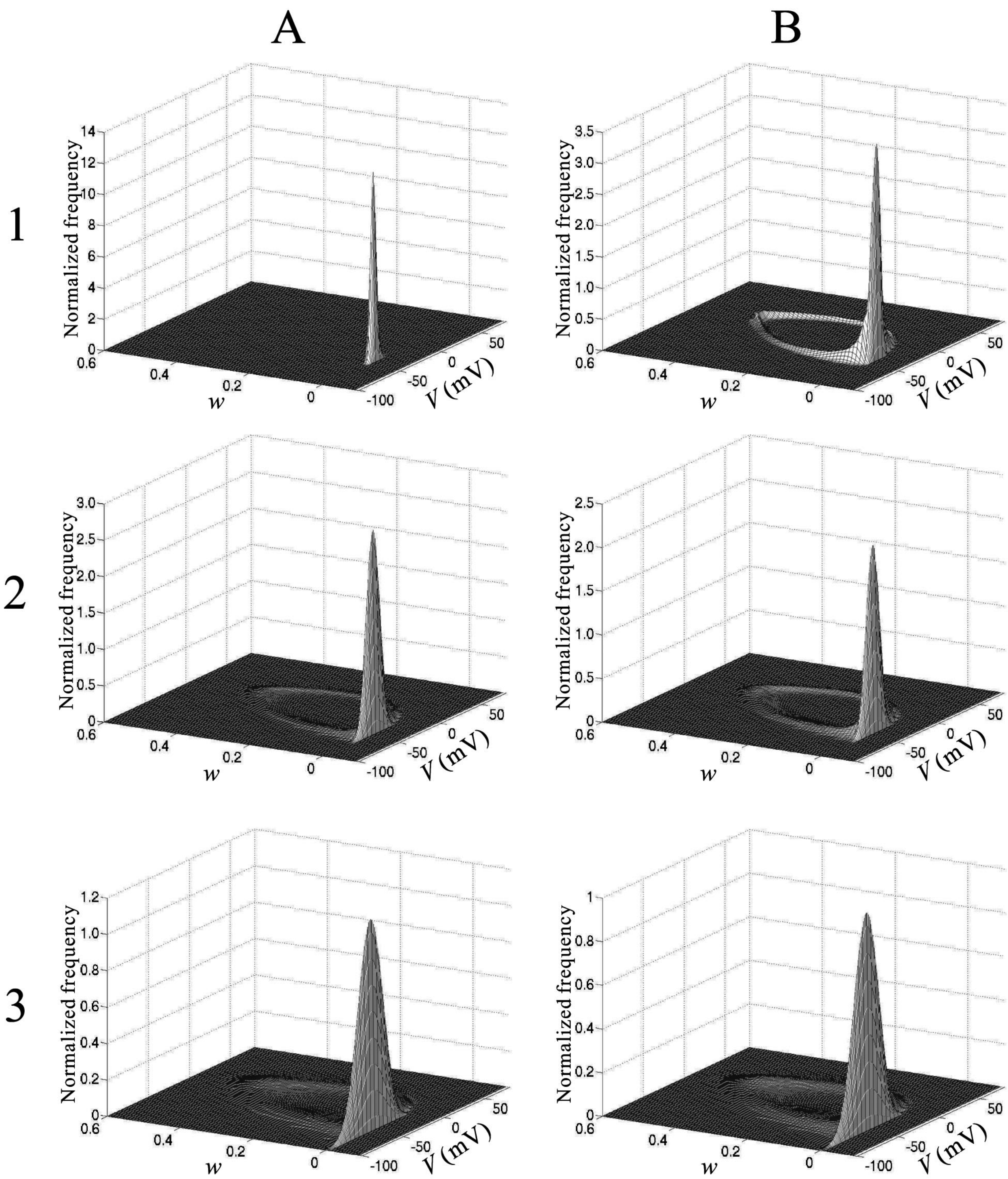

FIG. 4. Stationary distributions of the class I ML model in the excitable (column panels A) and oscillatory (column panels B) regimes near the saddle-node separatrix-loop bifurcation point ($I_c \simeq 40$) for three different values of noise intensity in row panels 1, 2, and 3. Parameters: (A) $I = 39.0$ (μA/cm^2) and (B) $I = 45.0$ (μA/cm^2). 1 $\sigma_0 = 0.5$, 2 $\sigma_0 = 3.0$, and 3 $\sigma_0 = 7.0$. The stationary distribution emerged as the three-dimensional histograms of the final position of all points in the v-w phase plane and normalized by the total number. The Heun scheme was used for the numerical calculation of Eq. (3) with a time step of $\Delta t = 0.001$. The numerical calculation was carried out for 10^9 time units after discarding the first 10^4 time units. More detailed explanation for the numerical calculation is described in the Appendix.

tem beyond the firing threshold (the stable manifold of the saddle point). At low noise levels, such escapes are extremely rare and they occur in general through the saddle point. So, besides the Gaussian-type peak centered on the stable equilibrium, the stationary distribution ρ presents also a ring like form going over the heteroclinic connections from the saddle point to the stable equilibrium point. At low noise levels, this ring is hardly visible, however, as the noise intensity is increased, it becomes more prominent, as, simultaneously, the peak of the Gaussian-type peak decreases and its width increases (panel A2 in Fig. 4). Further increase in the noise intensity magnifies these effects (panel A3 in Fig. 4), as both the dampened peak and the ring expand to wider regions as a consequence of wider noise induced fluctuations in the phase space.

When the ML model is oscillating, the low-noise stationary distribution takes on a ring-like shape over the limit cycle. At each cross section of the cycle, it has a Gaussian like form. However, the ring is not uniformly distributed along the cycle. It displays peaks and troughs (panel B1 in Fig. 4). The peaks represent the regions in which the dynamics along the cycle is slow, and, conversely, the troughs reflect the faster dynamics. As the noise intensity is increased, the differences between these tend to decrease, while, at the same time, the ring-like distribution widens and spreads further away from the vicinity of the limit cycle (panel B3 in Fig. 4).

The above descriptions suggest that, whether in the excitable or oscillating range, increasing the noise intensity, while producing quantitative changes in the stationary distributions, does not lead to any qualitative change. In other words, based upon the numerical explorations, one cannot conclude that there is a noise induced P-bifurcation in the system.

Similarly, it is possible to compare, at a fixed noise intensity, the shapes of the stationary distributions ρ for the excitable and oscillating class I ML model. Clearly, at large noise intensities, the shapes of ρ are qualitatively similar (compare panels A3 and B3 in Fig. 4). The low-noise densities are qualitatively similar to the large-noise densities. In other words, there are no P-bifurcations in the stochastic class I ML model, as one moves from the excitable to the oscillating range. Heuristically, this absence of P-bifurcations can be accounted for by considering that P-bifurcations are sometimes characterized as changes in the number of peaks of the stationary distribution ρ,[30] and that these peaks are indicators of regions in which the stochastic system spends most of its time. In the excitable range, the peak is situated at the stable equilibrium point. At the saddle-node loop bifurcation from excitable to oscillating regimes, the peak is at the saddle-node, where the dynamics are slowed down. Beyond the bifurcation, in the oscillating regime, the dynamics along the limit cycle is slowed down in the phase space region near to the former location of the saddle-node. Therefore, the stationary distribution ρ in the oscillating regime also presents a marked peak similar to the one observed in the excitable regime. In conclusion, despite the bifurcation of the deterministic system, the shape of the stationary distribution of the stochastic system does not undergo any qualitative change.

B. The stationary distribution in the class II regime

In this section, we describe stationary distribution properties of the class II ML model, focusing on the similarity and difference between the two classes. In the class II regime, the transition from the excitable state to the oscillating regime goes through a bistable regime, with coexisting stable equilibrium point and stable limit cycle, while it does not in the class I regime. When the current and noise intensities are set to be bifurcation parameters and others are fixed, stationary distributions of the class II ML model could basically be formed from one of (i) a peak around the equilibrium point, (ii) a surrounding ring reflecting the spike trajectory, or (iii) a composite of both as well as those of the class I ML model. In the presence of noise, however, there is no bistability in the sense that in all cases, i.e., excitable, bistable, and oscillating, the system admits a unique stationary distribution. In the case of the class I ML model, we have already argued that there was no evidence of P-bifurcations in the parameter ranges that we explored. For the class II ML model, the situation is more complex owing to the bistable regime. The numerical explorations we have performed do not rule out the occurrence of P-bifurcations. In the following, we depict some of the typical shapes of the stationary distribution we observed in the individual regimes of the class II ML model.

As stated above, the main similarity between the class I and class II ML models is that both exhibit excitatory and oscillatory regimes. Therefore, the shapes of the stationary distributions ρ of the class II stochastic ML model outside of the transition range (the bistable regime), that is, in the excitable and oscillating regimes, are reminiscent of those in the class I model (see panels A and B in Fig. 4 and compare with panels A and B in Fig. 5). Indeed, the distribution ρ has a peak and a surrounding ring-like hump. In the excitable regime, the latter becomes visible only at sufficiently large noise intensities. In the oscillating regime, the ring is on the action potential trajectories and the peak represents the region where the dynamics is slower.

In the bistable regime, the situation is more complex. One reason is the existence of metastable distributions at low noise levels. Indeed, at low noise levels, hopping between the stable equilibrium point and the stable limit cycle and vice versa may not occur within the simulation time. In such cases, simulations started at an initial condition close to the stable equilibrium point produce distributions that are Gaussian-like and centered at the equilibrium (panel A1 in Fig. 6), while those initiated in the vicinity of the limit cycle lead to a ring-like distribution (panel B1 in Fig. 6) such as the one in the oscillating regime. However, the stationary distribution is unique and independent from the initial distribution of points. Furthermore, due to noise induced hopping, one expects the stationary distribution to have both a peak around the equilibrium and a ring on the stable limit cycle. Therefore the distributions obtained numerically are not the stationary one, but metastable ones. They end up converging to the unique stationary distribution. However, the duration of this process tends to infinity as the noise intensity is decreased, so that practically, it is not possible to obtain the stationary distribution at arbitrarily low noise levels from numerical simulations of solution sample paths.

To avoid this problem that is proper to the bistable regime, we systematically computed the distribution for two initial conditions, one on the equilibrium and the other on the stable limit cycle. Only when both led to visually indistinguishable results, we considered them to represent a proper numerical estimate of the stationary distribution of the system. The rows in Fig. 6 represent numerical estimates of

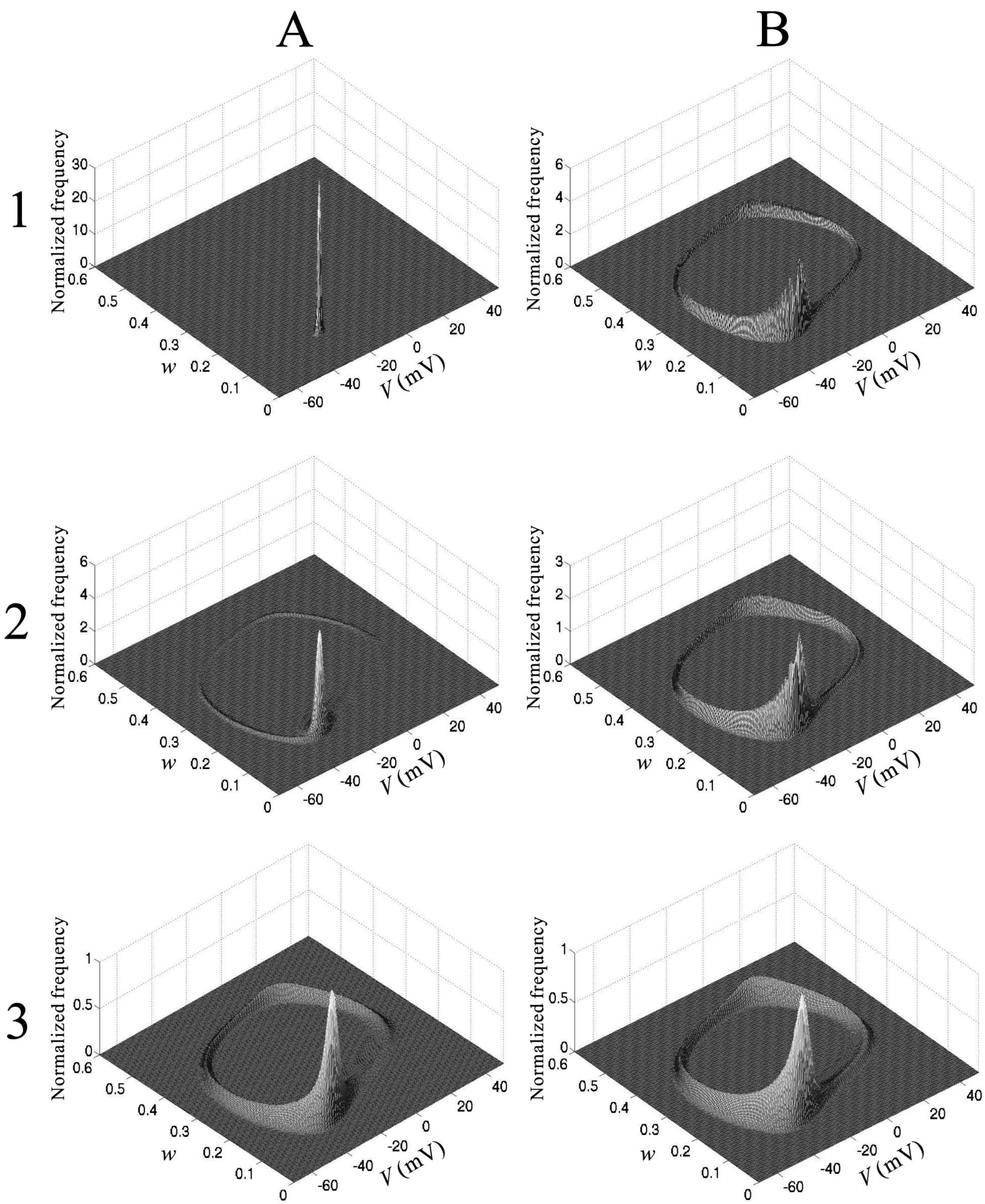

FIG. 5. Stationary distributions of the class II ML model in the excitable regime (column panels A) near the double-cycle bifurcation point ($I_{DC} \simeq 88.29$) and oscillatory regimes (column panels B) near Hopf bifurcation point ($I_H \simeq 93.86$) for three different values of noise intensity in row panels 1, 2, and 3. Parameters: (A) $I = 88.2$ (μA/cm^2) and (B) $I = 94.0$ (μA/cm^2). (1) $\sigma_0 = 0.2$, (2) $\sigma_0 = 0.5$, and (3) $\sigma_0 = 1.0$.

distributions obtained for fixed parameter sets but starting from the two different initial conditions situated on the equilibrium point and on the stable limit cycle. Besides the first row where the two distributions are clearly different, the others are similar.

As mentioned above, typical stationary distributions in the bistable regime present a peak on the stable equilibrium point and ring on the stable limit cycle. This ring itself is not uniform, and has a maximal value at the range where the cycle is slow. Therefore, we expect the stationary distribution

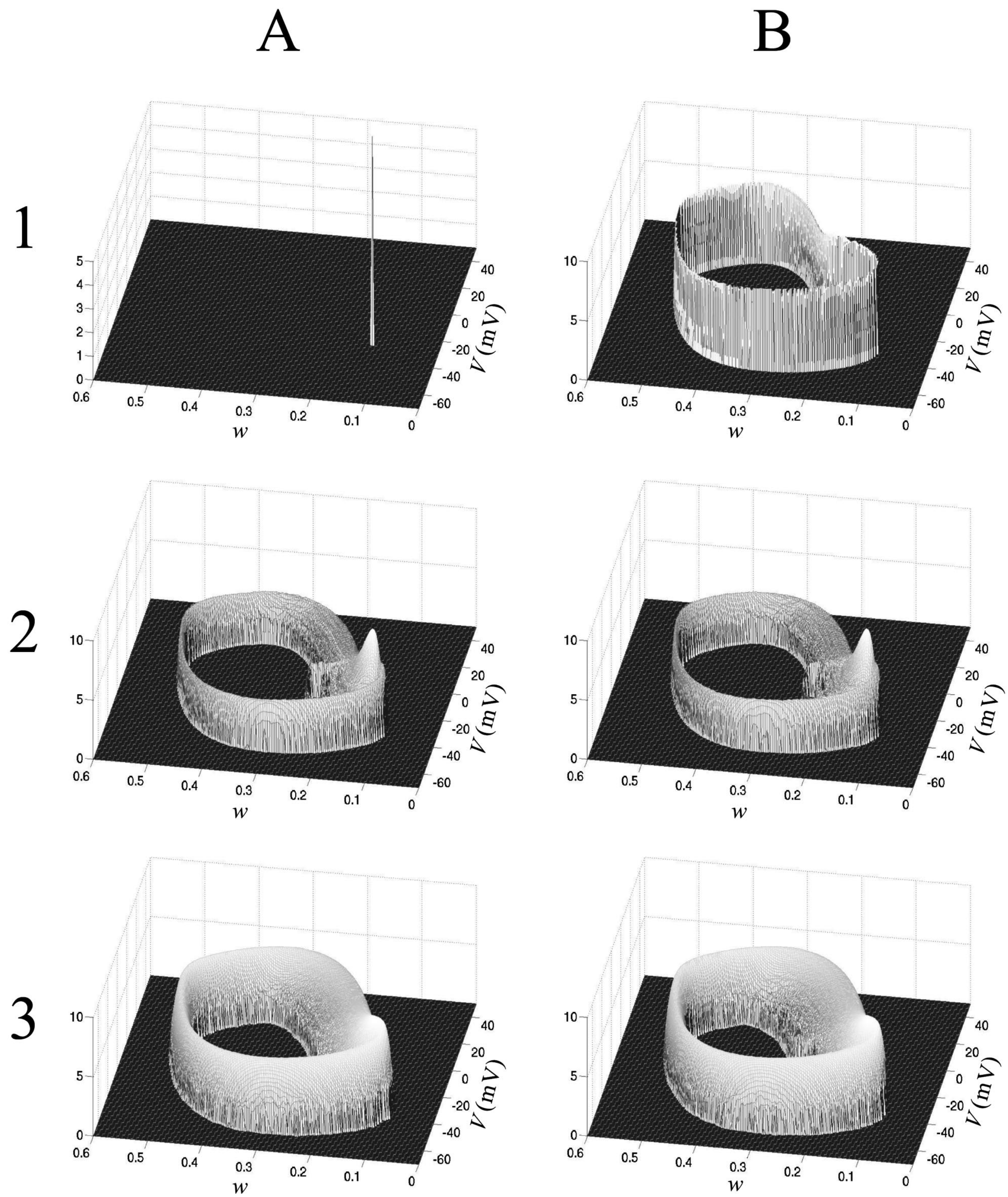

FIG. 6. Stationary distributions of the class II ML model in the bistable regime. The initial conditions were on the equilibrium point (column panels A) and the stable limit cycle (column panels B) for three different values of noise intensity in row panels 1, 2, and 3. In order to make small changes visible the logarithmic scale ($\log(1+z)$) on the vertical axis was used. Parameters: (A) and (B) $I=88.3$ (μA/cm^2). (1) $\sigma_0=0.0001$, (2) $\sigma_0=0.3$, and (3) $\sigma_0=0.8$.

to display distinct maxima, one associated with the peak at the equilibrium, and one associated with the maximal value around the ring (panels A2 and B2 in Fig. 6).

The distinction between the separate peaks is not possible when the noise intensity becomes large. Indeed, in this situation, noise induced hopping becomes frequent. The time spent by the system in tight vicinities of the equilibrium and the stable limit cycle is of the same magnitude as that spent going from one to the other as well as exploring wider regions of the phase space. The panels on the third row of Fig. 6 illustrate this phenomenon. In summary, the numerical estimates suggest that distinct maxima of the stationary distribution merge as the noise is increased. Such a change in the shape of the stationary distribution may be reminiscent of a P-bifurcation.

A similar merging of the maxima occurs at either end of the bistable regime, that is, at the double cycle and at the subcritical Hopf bifurcation. In the double cycle bifurcation, it is the maximum associated with the ring that approaches the hump over the equilibrium point, while, in the subcritical Hopf bifurcation, it is the peak associated to the equilibrium point that moves on the limit cycle. These changes can be observed as long as the noise intensity is too large. They may also be indicative of the occurrence of P-bifurcations in the model.

The examples shown in Fig. 6 depict the complicated changes observed in the stationary distributions in the bistable regime. These changes might be related to P-bifurcations. However, to our knowledge, there are no general and universally applicable analytical tools available that would permit us to confirm or invalidate this. Our aim in this paper is not to show an occurrence of the P-bifurcation, but to describe the qualitative difference between the class I and II regimes. This is clearly fulfilled with our analysis which establishes that (i) the stationary distributions in the excitable and oscillating regimes of class I and II ML models are fairly similar (ii) yet, there are marked differences in the shapes of these distributions and their dependence on model parameters and noise intensities, in the range of transition from excitability to oscillations.

V. THE RDS APPROACH

A method which is based only on the information obtainable from probability distributions of the solution X at $t \geqslant 0$ of a set of stochastic differential equations emanating from one arbitrary point X_0 is called a one-point method.[31] As we have already addressed, for example, a stationary distribution is a one-point object. Moreover, a notion obtained from the joint distribution of a pair of two points X and Y at which the two solutions are simultaneously found at time t for the corresponding initial points X_0 and Y_0 $(X_0 \neq Y_0)$ is referred to as a two-point notion. Similarly, a multiple-point notion or, even more, an infinite-point notion can be defined. In the above sense, roughly speaking, the stochastic description is based on the one-point notion while the RDS theory on a different approach, i.e., the multiple-point notion, as we will explain in more detail below.

The RDS theory considers noisy systems from a different standpoint. That is, the RDS theory analyzes the dynamics of different initial conditions under the same noise realization. Roughly speaking, the stochastic approach considers the dynamics of an initial condition (i.e., the one-point notion) under all possible noise realizations, while, RDS takes on the evolution of all initial conditions (i.e., the multiple-point notion) under one noise realization. In this way, for each noise realization, RDS studies the dynamics of a nonautonomous dynamical system. In principle, we have as many dynamical systems as noise realizations: to each noise realization there corresponds a different nonautonomous dynamical system. We thus have a family of non-autonomous dynamical systems. The random selection of the noise realization is in fact interpreted as the random selection of one system from this family. The noise realization can take on a variety of forms, so that it may seem an impossible task to analyze all systems within the family. However, remarkably, under wide conditions, for almost all noise realizations, the dynamics of the nonautonomous systems within the family will strongly resemble one another. This similarity makes it possible to describe typical dynamics for the family. In the following paragraphs, we provide a brief outline of RDSs and introduce key concepts that are used in our study. For a comprehensive treatment please refer to Arnold.[16]

In contrast to the one-point notion, an ordinary differential equation (ODE) $dx/dt = f(x)$ can generally generate a dynamical system, namely, a flow $(\varphi(t))_{t\in\mathbb{R}}$ for each x in an n-dimensional space $\mathbb{R}^n$. Briefly, a family $(\varphi(t))_{t\in\mathbb{R}}$ of self-mappings of a space is called a flow if it satisfies $\varphi(0) = \mathrm{id}$ and $\varphi(t+s) = \varphi(t)\circ\varphi(s)$ for all $s,t \in \mathbb{R}$, where $\circ$ denotes composition. The flow describes not just the one-point motion, but also the simultaneous motion of arbitrarily many points. In other words, the flow ''remembers'' not only all individual one-point motions, but also does the simultaneous motion of arbitrarily many points. The concept of the flow plays a central role in the analysis of deterministic dynamical systems. This concept is also able to extend to a stochastic version. In the RDS theory, the cocycle extends the concept of the flow to the case of systems undergoing random perturbations. For example, the stochastic processes are obtained by solving arbitrarily many copies of Eq. (3) with an identical Wiener process realization, but with all different initial conditions. This object is called a stochastic flow, and especially if, for each $x \in \mathbb{R}^n$, $s,t \in \mathbb{R}$, and all $\omega \in \Omega$, $\varphi_{st}(\omega,x)$ is a solution of a stochastic differential equation at time t in the interval $[s,\infty]$ with an initial point x at time $s<t$, it is called a two-parameter flow $(\varphi_{st}(\omega)) := (\varphi_{st}(\omega,\cdot))$. In the case, we also have the two-parameter flow property: for all $0 \leqslant s \leqslant r \leqslant t$ and all $\omega \in \Omega$,

$$\varphi_{ss}(\omega,x) = \mathrm{id}_{\mathbb{R}^n}, \quad \varphi_{st}(\omega) = \varphi_{rt}(\omega)\circ\varphi_{sr}(\omega), \tag{4}$$

where $\circ$ means composition. The construction of a flow $(\varphi_{st})_{s\leqslant t}$ from a stochastic differential equation is a big progress because $\varphi_{st}(\omega)$ can now be differentiated with respect to x, namely, φ_{st} is a diffeomorphism, and its geometry can be analyzed. For more precise conditions and the general theory of stochastic flows we refer the reader to the book by Kunita.[32] A stochastic flow φ_{st} is still a static object and not yet a (random) dynamical system. That is, for each ω the family $(\varphi(\omega))_{0\leqslant s\leqslant t}$ of diffeomorphisms of $\mathbb{R}^n$, where n is an integer, is a deterministic two-parameter flow in the sense that ω is frozen. At this point, however, the flows for different ω's are not related to each other. Such a relation appears when we try to suppress one time argument in the two-parameter flow property of Eq. (4) by putting $s=0$. To do this, we need to describe the driving Wiener process as a dynamical system. In other words, before we proceed to the explanation of the cocycle, a metric dynamical system which models the white noise is needed because an RDS or a cocycle consists of two basic ingredients: a model of the noise and a model of the system which is perturbed by the noise.

Let $(W_t)_{t\in\mathbb{R}}$ be the standard Wiener process in $\mathbb{R}$ with $W_0=0$. Put $\Omega=\{\omega|\omega\in\mathcal{C}(\mathbb{R}),\omega(0)=0\}$, $\mathcal{F}$ the Borel σ-algebra of Ω, $\mathbb{P}$ the (Wiener) measure on $\mathcal{F}$ generated by W. The shift on Ω is defined as $\theta_t\omega(s):=\omega(t+s)-\omega(t)$. Then θ is an ergodic metric dynamical system on the triplet $(\Omega,\mathcal{F},\mathbb{P})$, and $W_t(\omega)=\omega(t)$ is Brownian motion. Next, we define a cocycle which models the system perturbed by the white noise. Let $(\Omega,\mathcal{F},\mathbb{P},(\theta_t)_{t\in\mathbb{R}})$ be a metric dynamical systems defined above. Let

$$\varphi:\mathbb{R}\times\Omega\times\mathbb{R}^n\to\mathbb{R}^n,\quad (t,\omega,x)\mapsto\varphi(t,\omega,x) \tag{5}$$

be a mapping with the following properties:

(i) $\varphi(0,\omega)=\mathrm{id}_{\mathbb{R}^n}$,

(ii) for all $s,t\in\mathbb{R}$ and all $\omega\in\Omega$,

$$\varphi(t+s,\omega)=\varphi(t,\theta_s\omega)\circ\varphi(s,\omega), \tag{6}$$

where $\circ$ denotes composition of mappings.

The second is called a cocycle property. Note that $\varphi(t,\omega)x=\varphi_{0t}(\omega,x)$ $(t\geqslant 0)$.

One of the basic objects of interests in dynamical systems is an invariant measure. For instance, the analysis of the long term dynamics of deterministic systems goes through the determination of equilibria, limit cycles, etc. In other words, the long term analysis examines structures that remain invariant under the deterministic flow. An invariant measure ρ for the flow φ generated by an ODE $dx/dt=f(x)$ is defined by $\varphi(t)\rho=\rho$ for all $t\in\mathbb{R}$. Notice that if ρ is a measure and φ a measurable mapping, then $\varphi\rho$, the image of ρ under φ, is the measure defined by $\varphi\rho(\cdot)=\rho(\varphi^{-1}(\cdot))$. In addition, the infinitesimal form of the invariant measure is *Liouville's equation* $\mathrm{div}(\rho f)=0$.

Since the stochastic analog of the Liouville's equation is the Fokker–Planck equation, it seems quite natural to define an invariant measure of an SDE as one which solves the Fokker–Planck equation $L^*\rho=0$, where L^* is an operator of the Fokker–Planck equation of the corresponding SDE. In the RDS theory, this is actually the point of view called a stationary measure rather than an invariant measure. The stationary measure plays a prominent role in applications, because it is the one that is in general practically observable. In the context, a probability measure ρ on $(\mathbb{R}^d,\mathcal{B}^d)$, where $\mathcal{B}^d$ is the Borel sets in $\mathbb{R}^d$, is called stationary for an SDE if it is invariant under $P(t,x,\cdot)$ and satisfies the relation

$$\rho(\cdot)=\int_{\mathbb{R}^n}P(t,x,\cdot)\rho(dx)\quad\text{for all}\quad t>0, \tag{7}$$

where $P(t,x,\cdot)$ is a transition probability, i.e., $P(t,x,B)=\mathrm{P}\{X_t\in B|X_0=x\}$, which is related with a Markov process X_t generated by the SDE. The stationary measure is clearly a one-point object. The value $\rho(B)$ gives the proportion of time a solution X_t of the SDE with a initial value x spends in the set B.

In the RDS theory, however, there exists a second possibility to extend the deterministic definition which seems to be equally natural, but more general. The RDS analysis thus follows another approach, as it is concerned with the determination of random invariant measures. Let φ be an RDS. A random probability measure $\omega\mapsto\mu_\omega$ on $(\mathbb{R}^d,\mathcal{B}^d)$ is said to be invariant under φ if for all $t\in\mathbb{R}$

$$\varphi(t,\omega)\mu_\omega=\mu_{\theta_t\omega}\quad \mathbb{P}\text{-a.s.}, \tag{8}$$

where P-a.s. denotes P almost surely. The concept of a stationary measure given by Eq. (7) is older and more restrictive than that of an invariant measure for the RDS φ generated by the corresponding SDE. However, there exists a one-to-one correspondence between the stationary measure ρ, and a special random invariant measure, denoted by μ_ω referred to as Markov invariant measures

$$\rho\mapsto\mu_\omega:=\lim_{t\to\infty}\varphi(t,\theta_{-t}\omega)\rho,\quad \mu_\omega\mapsto\rho:=\mathbb{E}[\mu], \tag{9}$$

where $E[\cdot]$ represents an expectation operator.

In deterministic dynamical systems, the local stability of equilibria is assessed through the spectral theory of matrices, which provides us with eigenvalues and eigenspaces. Briefly, in studies of the so-called local theory, stability of the deterministic dynamical system φ generated by an ODE $dx/dt=f(x)$ with $f(0)=0$ in a neighborhood of 0 is based on the simple fact that the dynamics of the linearized dynamical system $\Phi(t)=(\partial/\partial x)\,\varphi(t,x)|_{x=0}$, i.e., the linear ODE $dv/dt=Df(0)v$, is completely determined by the computation of eigenvalues of the Jacobian matrix $Df(0)$. In the RDS theory, it is known that there indeed exists a stochastic version of spectral theory for the linearization $D\varphi(t,\omega,x)$ of a cocycle φ, but not just at a fixed point, but for a general reference solution under a φ-invariant measure μ. The multiplicative ergodic theorem proved by Oseledets (1968)[33] provides us with exactly the right kind of objects which one needs for local theory in RDSs. Moreover, the theorem is the basis for studying the long-term behavior of deterministic nonlinear systems by means of the exponential growth rates, namely, Lyapunov exponents, of the solution the variational equation (linearization). For an RDS, the local stability of random invariant measures is thus determined by their associated Lyapunov exponents. Based on the multiplicative ergodic theorem of Oseledets,[33] these are defined as follows:

$$\lambda(\omega,x,v):=\lim_{t\to\infty}\frac{1}{t}\log\|D\varphi(t,\omega,x)v\|, \tag{10}$$

for $v\neq 0$.

Dynamical stochastic bifurcations, denoted by D-bifurcations, are generally defined as qualitative changes in the stochastic phase portraits associated with the cocycle. Similarly to the case of deterministic dynamical systems whereby sign changes of (real parts of) eigenvalues of the Jacobian matrix at an equilibrium characterize local bifurcations, local D-bifurcations are associated with sign changes of Lyapunov exponents.

The implication of the above considerations for the ML model is that, practically, the analysis of the random dynamics of the system requires mainly the numerical estimation of the Lyapunov exponents of the system. Notably, one is concerned with potential sign changes of the exponents in the vicinity of the bifurcations of the deterministic system.

VI. NUMERICAL RESULTS ON THE RDS APPROACH

The Gaussian white noise input acts as an additive perturbation to the ML model, in the sense that it leaves no solution of the deterministic system invariant. As argued by Arnold *et al.*,[18] this makes it impossible to directly apply the analytical methods of stochastic bifurcation theory. In such cases, one needs to carry out careful numerical analysis of the dynamics of the system. This is the approach that we adopted. The tools used in the numerical exploration of RDSs are essentially the estimation of Lyapunov exponents, rotation numbers and the pullback and backwards random attractors. We describe these for the ML model in the following sections.

A. Lyapunov exponents

As mentioned above, sign changes in Lyapunov exponents associated with random invariant measures are indicators of D-bifurcations. In this section, we report how the Lyapunov exponents of the ML model in the class I and class II regimes vary with the constant current and the noise intensity.

The stochastic ML model possesses two Lyapunov exponents $\lambda_1 \geqslant \lambda_2$ which are exponential growth rates of a solution of the linearization (variation equation) corresponding to Eq. (3). The leading Lyapunov exponent λ_1 can actually be calculated as the following exponential growth rate:

$$\lambda_1 = \lim_{t\to\infty} \frac{1}{t} \log\|V(t)\|, \tag{11}$$

where $V(t)=(v_t, w_t)$ is a solution of the variation equation associated with Eq. (3) for any deterministic initial values except the origin. Practically, we estimated the leading Lyapunov exponent by the method described in the Appendix.

As for the deterministic dynamics and for the stochastic analysis, we describe successively the Lyapunov exponents in the class I and then in the class II regimes.

1. Class I regime

Before discussing the Lyapunov exponents of the stochastic ML model, it is appropriate to discuss how these quantities vary in the deterministic excitable and oscillating ranges, and the transition between the two.

In the excitable range, the Lyapunov exponents of the ML model equal the eigenvalues of the Jacobian matrix evaluated at the stable equilibrium point. Therefore, they are both negative, and the leading exponent tends to zero as the parameter I approaches the critical value at which the saddle-node loop bifurcation occurs. At this critical point, the leading exponent vanishes while the second exponent remains negative. Beyond the bifurcation point, i.e., in the oscillating range, the Lyapunov exponents equal the Floquet eigenvalues of the stable limit cycle. Therefore, the leading exponent remains zero, reflecting the neutral stability of the limit cycle to perturbations along the cycle. Conversely, the second exponent is negative reflecting the stability of the cycle against transversal perturbations.

The exponents of the stochastic ML model tend to those of the deterministic system as the noise intensity approaches zero. The upper panel (a) in Fig. 7(A) where Lyapunov exponents of the class I ML model at different values of I are represented against the noise intensity σ_0 illustrates this point. At the two lower values of I, namely $I=30$ and 38.5, for which the system is excitable, the leading exponent tends to the deterministic value as $\sigma_0 \to 0$. These two values correspond to the largest eigenvalue of the Jacobian matrix evaluated at the stable equilibrium point. For the two larger values of I, namely $I=40$ and 50, for which the system is oscillating, the exponents tend to zero, as expected.

The exponents at intermediate and large noise intensities depend on the dynamics of the deterministic system. When I is fixed in the excitable regime and σ increases, the Lyapunov exponents first increase, then have a certain maximum value at some noise intensity, and decrease [e.g., a curve labeled with $I=38.5$ in Fig. 7(Aa)]. Throughout, the exponent remains negative. In the oscillatory regime, with increasing noise intensity, the Lyapunov exponents monotonically decrease. The same holds at the critical value at which the deterministic system undergoes the saddle-node loop bifurcation. The main difference between the leading Lyapunov exponent in the oscillating regime and at the bifurcation point is observed in the slope of the curve at $\sigma_0 = 0$. In the oscillating regime, the slope is zero, while, at the bifurcation point, it takes on a negative value.

Despite the differences in the shapes of the curves representing the leading Lyapunov exponent against the noise intensity for different values of I, one observation common to all the cases is that the exponent is negative for all $\sigma_0 > 0$. This is clearly apparent when the Lyapunov exponents are represented in I-σ parameter space [Fig. 7(Ab)]. The absence of sign changes in the leading Lyapunov exponent suggests that there are no D-bifurcations in the class I stochastic ML model, or, in other words, that additive noise destroys the bifurcation of the deterministic system.

2. Class II regime

In the class II regime, the Lyapunov exponents of deterministic ML model in the excitable range are both to the (negative) real part of the pair of complex conjugate eigenvalues of the Jacobian matrix of the system at the equilibrium point. In the oscillating range, similarly to the class I regime, the exponents equal the Floquet eigenvalues of the limit cycle, so that the leading one is zero and the second one is negative. In the transition range, the system is bistable, so that it possesses two pairs of Lyapunov exponents, one associated with the stable equilibrium point and the other with the stable limit cycle.

In the same way as for the class I ML model, in the excitable and oscillating regimes, the leading Lyapunov exponent of the system tends to the deterministic value(s) as $\sigma_0 \to 0$. In the bistable range, the stochastic system, unlike the deterministic one, has only a single pair of Lyapunov exponents. At low noise levels, these exponents tend those of the equilibrium when the system is near the double cycle bifurcation, and conversely to those of the limit cycle, when the system is near the subcritical Hopf bifurcation. This observation is in agreement with that of the stationary distribution ρ reported previously. Indeed, even though in the

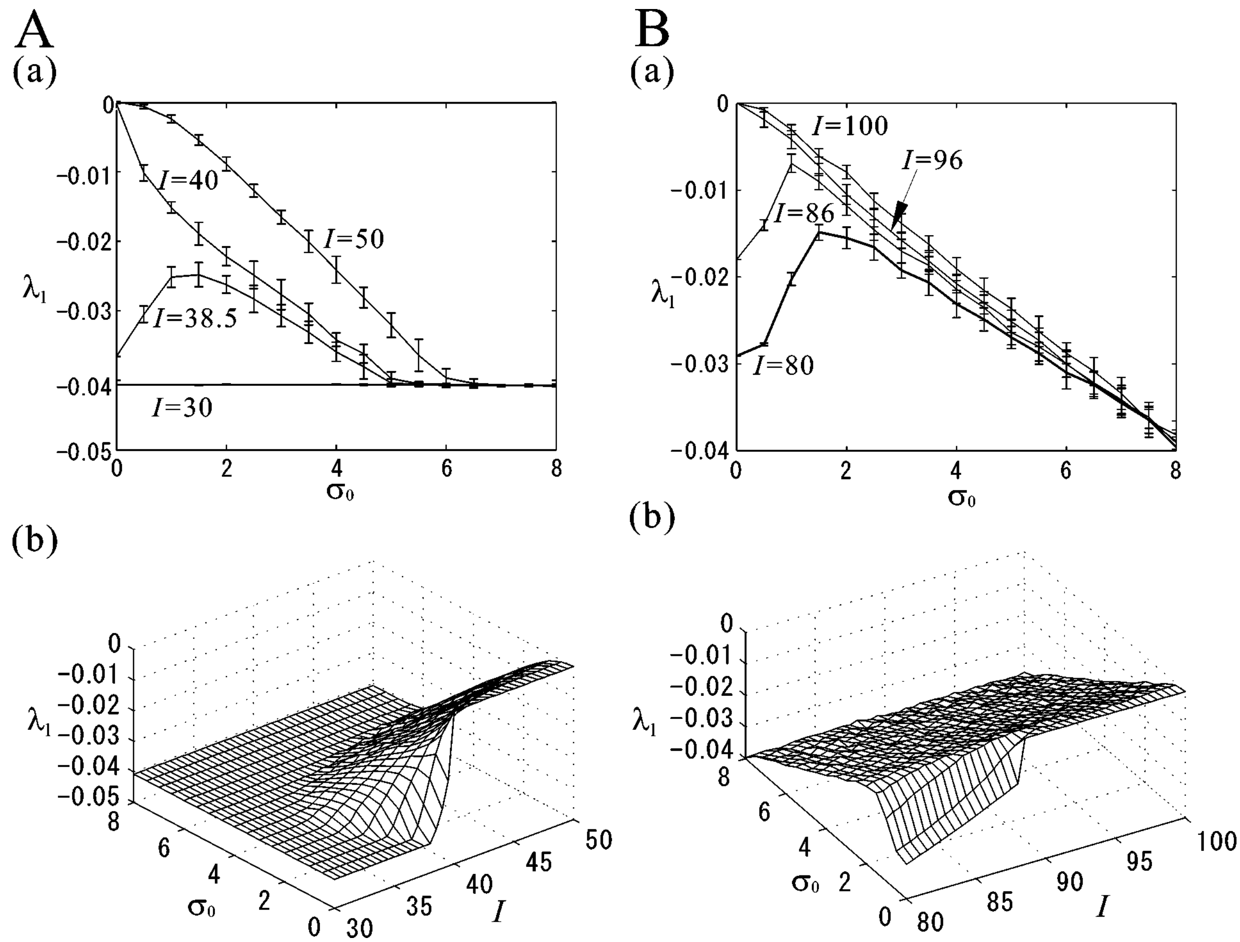

FIG. 7. Leading Lyapunov exponents of the stochastic ML model. (A) The class I ML model. (a) Mean values and standard deviations of the leading Lyapunov exponents are shown against noise intensity for four different current values ($I=30$, 38.5, 40, and 50 μA/cm^2). The former two are in the excitable regime and the latter the oscillatory regime. The Lyapunov exponents were calculated for 20 different noise realizations each time with the noise intensity $\sigma_0(=\sigma/C)$ ranging from 0 to 8 with a step of 0.5. (b) Averaged leading Lyapunov exponents λ_1 on the parameter plane I-σ_0. The Lyapunov exponents were calculated in the same way as part (a). (B) The class II ML model. (a) Mean values and standard deviations of the leading Lyapunov exponents against noise intensity for four different current values ($I=80$, 86, 96, and 100 μA/cm^2). The former two are in the excitable regime and the latter two in the oscillatory regime. The Lyapunov exponents were calculated as the same way as column **A** with the noise intensity σ_0 ranging from 0 to 8 with a step of 0.5. (b) Averaged leading Lyapunov exponents λ_1 on the parameter plane I-σ_0.

bistable range the system hops from the vicinity of the equilibrium to that of the stable limit cycle, and vice versa, the relative times spend in the two neighborhoods strongly depend on system parameters. Close to the double cycle bifurcation, the system is mainly confined to the neighborhood of the equilibrium, while close to the subcritical Hopf bifurcation, the opposite holds, that is, the system remains mostly in the neighborhood of the limit cycle. This asymmetry accounts for the differences in the low noise evolutions of the Lyapunov exponents at either end of the bistable range.

The low noise estimation of the Lyapunov exponents is hindered by the metastable regimes in the same way as the estimation of the stationary distribution ρ. To make sure that the estimates corresponded to the regime once the metastable transients have ended, the Lyapunov exponents were estimated from an initial condition at the equilibrium and another one situated on the limit cycle.

Figure 7(B) shows the Lyapunov exponents of the class II ML model. As shown in Fig. 7(Ba), for four fixed current intensities in the excitable and oscillatory regimes, the tendency of the changes of the Lyapunov exponents in the class II ML model is similar to that in the class I ML model. More precisely, in the oscillating regime, the leading exponent decreases monotonically as the noise intensity is increased, while, in the excitable regime, the Lyapunov exponent presents a hump at some intermediate noise level. Overall, as shown in Fig. 7(Bb), the Lyapunov exponents are always negative in an I-σ parameter space. Consequently, in the same way as in the class I regime, there are no D-bifurcations in this system: additive noise destroys the bifurcations (both the double cycle and the subcritical Hopf bifurcations) of the deterministic system.

B. The attractor of the stochastic ML model

Our analysis of the D-bifurcations of the ML model was based upon the computation of the Lyapunov exponents. Indeed a sign change in the Lyapunov exponents of the system is an indicator of a qualitative change in the Markov invariant measure. We detected no such sign changes and therefore concluded that no D-bifurcations take place in the ML model, whether of class I or class II. In this section, we continue this analysis by computing the support of the Markov random invariant measure. The numerical investigations reveal that it is in fact reduced to a single point.

The fundamental relation in the computation of the support of the Markov random invariant measure is Eq. (9) that establishes the relation between the stationary distribution ρ and the Markov random invariant measure. Notably, the left-hand relation in Eq. (9) shows how one can derive the random invariant measure from the stationary distribution. This procedure is referred to as the pullback method. Indeed, it consists in initiating the system with points distributed according to the distribution ρ at some time $t=t'<0$ "in the past," and letting it evolve to the present time $t=0$ under the influence of the noise realization ω. The outcome at $t=0$ is a measure that is random (i.e., it depends on the noise realization) and that depends on the start time t'. As the initial starting time t' is pulled back in time towards $-\infty$, this random measure tends to the Markov random invariant measure (in the sense of weak convergence).[16]

We denote by $A(\omega)$ the support of Markov random invariant measure. This notation emphasizes the fact that the set $A(\omega)$ is in fact a random set, and to different noise realizations ω and ω' may correspond different sets $A(\omega)$ and $A(\omega')$. The fact that the Lyapunov exponents of the system are negative imposes that (i) for almost all ω, $A(\omega)$ is composed of finite number n of points, with n being independent of ω, and furthermore that (ii) except for possibly an ω dependent set of initial conditions of Lebesgue measure zero, trajectories of initial conditions x approach A in the sense that, for almost all ω,[34]

$$\lim_{t\to+\infty} \mathrm{dist}[\varphi(t,\omega,x),A(\theta_t\omega)]=0, \tag{12}$$

where $\mathrm{dist}[\varphi(t,\omega,x),A(\theta_t\omega)]$ denotes the distance between $\{\varphi(t,\omega,x)\}$ and $A(\theta_t\omega)$ and equals the minimum of the n distances between the point $\varphi(t,\omega,x)$ and the n points in $A(\theta_t\omega)$. In this way, the random set $A(\omega)$ plays the role of an attracting set for the system.

Practically, using the pullback method, we estimated the attracting set $A(\omega)$ for the stochastic ML model in different regimes and for different parameter values. In all cases we obtained that $A(\omega)$ was reduced to a single point, that is, $n=1$. Figure 8 illustrates one example of the derivation of $A(\omega)$. It represents different stages of the pullback procedure for the class II ML model in the oscillatory regime with a noise intensity $\sigma=2.0$. The initial conditions of the pullback are spread according to a regular rectangular grid on the plane [Fig. 8(A1)] rather following the stationary distribution ρ. As the initial time at $t=t'$ runs back to the negative direction, the formation of all points shrinks to a narrower region at $t=0$ in the phase space. In the figure, the region where each state point is scattered forms a loop and includes a vicinity of the deterministic equilibrium point and the ring-like spike trajectory. As the initial time is progressively moving back in time, the region becomes a formation consisting of a thinner loop and concentrated points around the equilibrium point as shown in Figs. 8(A2) and 8(B2). As the initial time is moved even further back in time, the set of points forms a formation of some arcs and a concentrated region [Fig. 8(A3)]. With t' further back in time, the points cluster in either the vicinity of the equilibrium point or parts of a loop around it as shown in Fig. 8(B3), and eventually they all collapse into a single tight group where they cannot be visually distinguished from one another. This tight group can be assimilated to a single point. It remains invariant under pulling further back the time. In this way, it represents the numerical estimate of the set $A(\omega)$ and shows that this set is composed of a single point, that we denote by $(v^*(\omega),w^*(\omega))$. In fact $(v^*(\theta_t\omega),w^*(\theta_t\omega))$ is a stationary stochastic process, that is referred to as a stochastic equilibrium point.[16] From the limit (12), we derive that for almost all noise sample path ω, the trajectories of initial conditions, except for possibly a set of measure zero, tend to this unique stationary stochastic process.

Even though the possibly nonempty set of initial conditions whose trajectories do not converge to the stochastic equilibrium point has measure zero, it can bear some influence on the dynamics of the system. The excitable class I and class II ML models illustrate this point. In the former, trajectories initiated on the zero-measure closure of the stable manifold of the saddle point do not converge to the stable equilibrium point. Conversely, in the latter, that is the excitable class II ML model, all trajectories, with no exception, converge to the stable equilibrium point which is globally asymptotically stable. Clearly, it is the difference of the dynamics on a set of measure zero that permits the separation of class I and class II systems. The issue here is whether this difference persists in the stochastic models. More precisely, there is a difference between the basins of attraction of the stable equilibria of the deterministic excitable class I and class II ML models, and the corresponding stochastic ML models may inherit this difference. Such a difference in terms of the dynamics on a set of measure zero would not bear any influence on the previous results concerning the estimation of the Lyapunov exponents, rotation numbers or the support of the Markov invariant measure. However, in the deterministic case, this difference lies at the basis of the distinction between class I and class II membranes, so that it could be of biological interest to investigate whether it is also present in the stochastic ML model.

The origin of the difference between the excitable class I and class II membranes lies in the fact that the latter possesses a single equilibrium point while the former possesses three equilibria, two of which are unstable. Our investigations have indicated that whether in class I or class II regimes, and irrespective of the deterministic dynamics, the stochastic ML model possesses always a single stable stochastic equilibrium. However, these investigations focused on the Markov random invariant measure, and the system may possess non-Markov random invariant measures. These would play a role similar to that of the saddle and unstable source equilibrium points in the deterministic system. The issue is to determine whether such random invariant measures exist in the stochastic ML model.

The numerical determination of the equilibria of deterministic systems can be readily done by computing the zeros of the corresponding vector field. However, for stochastic systems with additive noise such as the stochastic ML model,

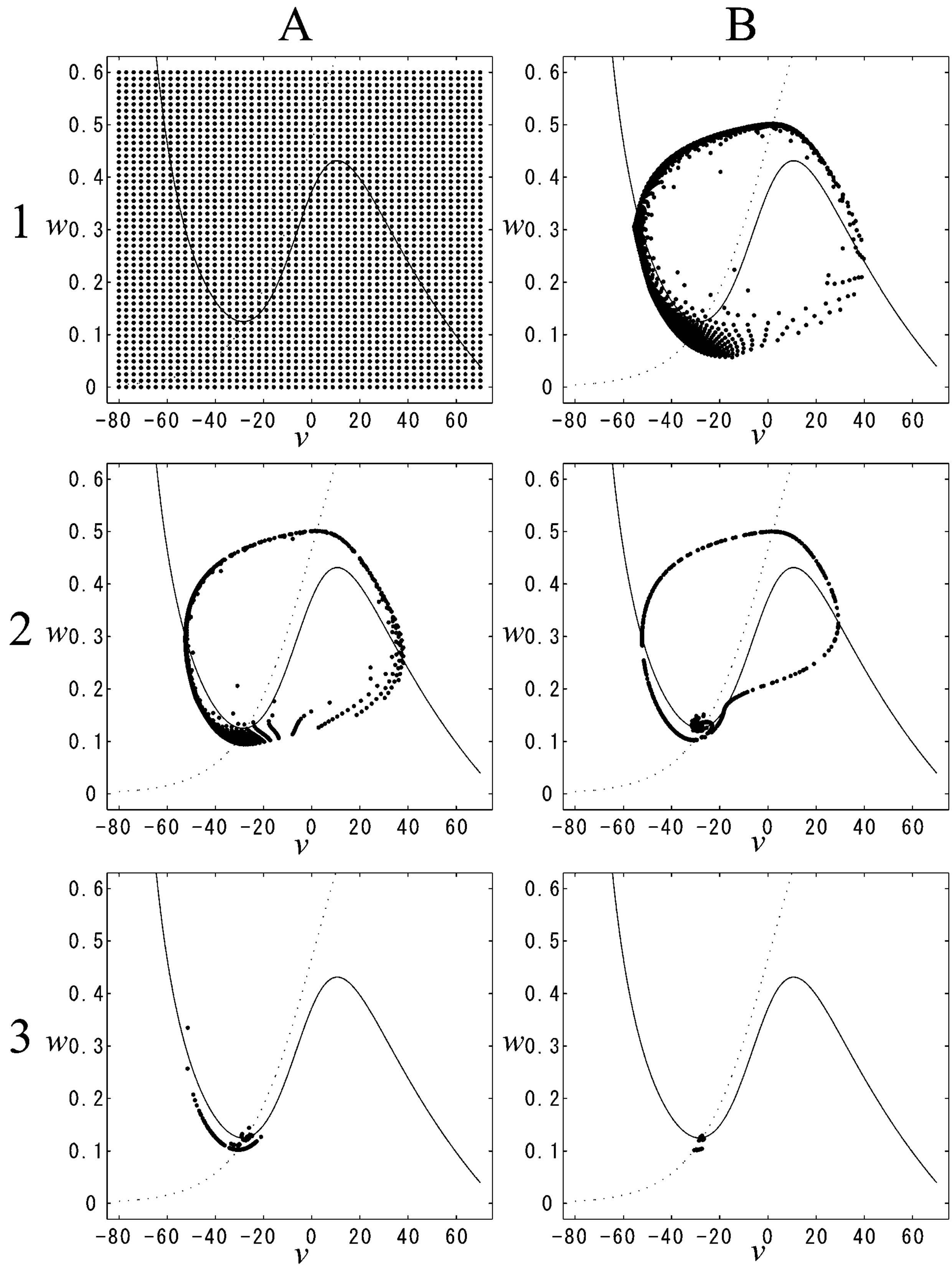

FIG. 8. Pullbacks of the stochastic class II ML model in the oscillatory regime for $I=88.4$ (μA/cm^2). For $\sigma=2.0$ snapshots of the state points at $t=0$ are illustrated in the phase space for a starting grid of 2500 initial conditions regularly positioned in rectangular grids at $t'=0$ ms (A1), at $t'=-20$ ms (B1), $t'=-30$ ms (A2), $t'=-200$ ms (B2), $t'=-450$ ms (A3), and $t'=-700$ ms (B3).

there is no such simple procedure. Besides the pullback method that yields the support of the Markov invariant measure, there are no systematic methods to directly compute random invariant measures. Arnold *et al.*[18] have used a method to overcome this. This consists in analyzing the time-reversed system. If for almost all ω, the time-reversed trajectories of initial conditions except possibly on a set of measure zero become unbounded, then one can argue that the time-reversed system does not possess any Markov random invariant measure. This procedure rules out the existence of random invariant measures that would play a role similar to an unstable source (node or focus) in the time-forward system. While it does not necessarily bear any indication on the existence of saddles, it provides extra information on the stochastic phase portrait of the system. We applied the time reversed procedure to the stochastic ML system. We initiated trajectories on a regular rectangular grid, and for each computed the time-reversed trajectory under the influence of the same noise sample path. We assumed that a solution would eventually become unbounded if the modulus of its voltage v became larger than a certain bound. Numerical simulations were performed in different regimes and with different noise intensities. In all cases, all computed trajectories went eventually out of the computation bound. From this result, we suggest that the time-reversed stochastic ML model does not possess any Markov random invariant measure.

The numerical explorations reported above suggest that there are no random invariant measures "stable with respect to the future." The case of saddle random invariant measures remains open. However, we conjecture that they do not exist in the parameter ranges that were explored numerically. In other words, we suggest that for almost all noise realizations the stochastic equilibrium of the ML model attracts trajectories of *all initial conditions*. In this sense, we argue that noise destroys the bifurcation scenario of the class I and class II regimes, and furthermore that there is no difference in terms of the asymptotic random dynamics of the two regimes.

C. Rotation numbers

The systematic numerical estimations of the Lyapunov exponents of the ML model in either class I or class II regimes reveal that, despite the bifurcations of the deterministic system, no D-bifurcations take place in the random system. Further analysis indicates that in fact in all explored situations, for almost all noise realizations, all trajectories eventually stabilizes at a uniquely defined stationary stochastic process. This indicates that from the RDS standpoint noise obliterates the differences that exist between the different regimes of the deterministic system. Despite this effect of noise, noise-induced changes are present in the system. Indeed, the stochastic equilibrium, unlike deterministic equilibria, displays dynamics. The stochastic equilibrium is a stationary stochastic process. The second relation in Eq. (9) *in general* shows that its distribution at a fixed time is given by the stationary distribution ρ, and can therefore undergo P-bifurcations. In this section, we investigate the changes in this stationary stochastic process with a different tool, namely the rotation number. The computation of the rotation numbers associated with the system provides information on noise-induced changes that are not necessarily associated with D-bifurcations. Such information cannot be gleaned from the Lyapunov exponents of the system. In this sense, the rotation numbers provide complementary information on the dynamics of the noisy system.

Rotation numbers are defined as

$$\gamma = \lim_{t\to\infty} \frac{1}{t} \arctan \frac{w_t}{v_t}, \tag{13}$$

where (v_t, w_t) is a solution of the variation equation associated with Eq. (3) for any deterministic initial values except the origin.

To clarify the interpretation of the rotation number and the origin of its denomination, it is helpful to first consider two deterministic situations. For a deterministic system stabilizing at an equilibrium point, the rotation number equals the imaginary part of the eigenvalues of the Jacobian matrix at the equilibrium. Conversely, when the deterministic system stabilizes at a limit cycle, the rotation number is the average angular velocity of the movement along the cycle.

With these interpretations in hand, we see that we have a clear difference between rotation numbers of deterministic class I and class II membranes. For class I membranes, the rotation number is zero in the excitable regime, and then increases continuously from zero after the transition from excitable to oscillating regimes. In this sense, the rotation number follows the evolution of the firing rate of the deterministic class I membrane. In class II membranes, the situation in the oscillating regime is similar to that of the class I membrane: the rotation number reflects the firing rate of system. However, in the excitable regime, the situation is different. The rotation number takes on a non zero value equal to the imaginary part of the complex conjugate eigenvalues of the Jacobian matrix. Finally, in the bistable range, we have two rotation numbers, one associated with the imaginary part of the eigenvalue of the Jacobian matrix at the stable equilibrium and the other related to the firing rate on the stable limit cycle.

The addition of noise alters the picture depicted above in several ways. In the stochastic ML model, the rotation number is uniquely defined, and its value does not depend on the choice of the initial condition. Furthermore, the value is the same for almost all noise sample paths. In this sense, we can discuss about *the* rotation number of the stochastic ML model. In the following we discuss the dependence of the rotation number on noise intensity in the different regimes and membrane classes.

The influence of noise on the rotation number in the oscillating regime is consistent with noise-induced changes in the firing rate of the system. In both class I and class II regimes, noise accelerates the firing rate of the ML model. Concurrently, the rotation number increases with the noise intensity σ.

In the excitable regime, the situation is more complex. At low noise intensities, when action potentials are rare, the rotation number is an indicator of the rate of subthreshold noise induced oscillations. At low noise intensities, the rota-

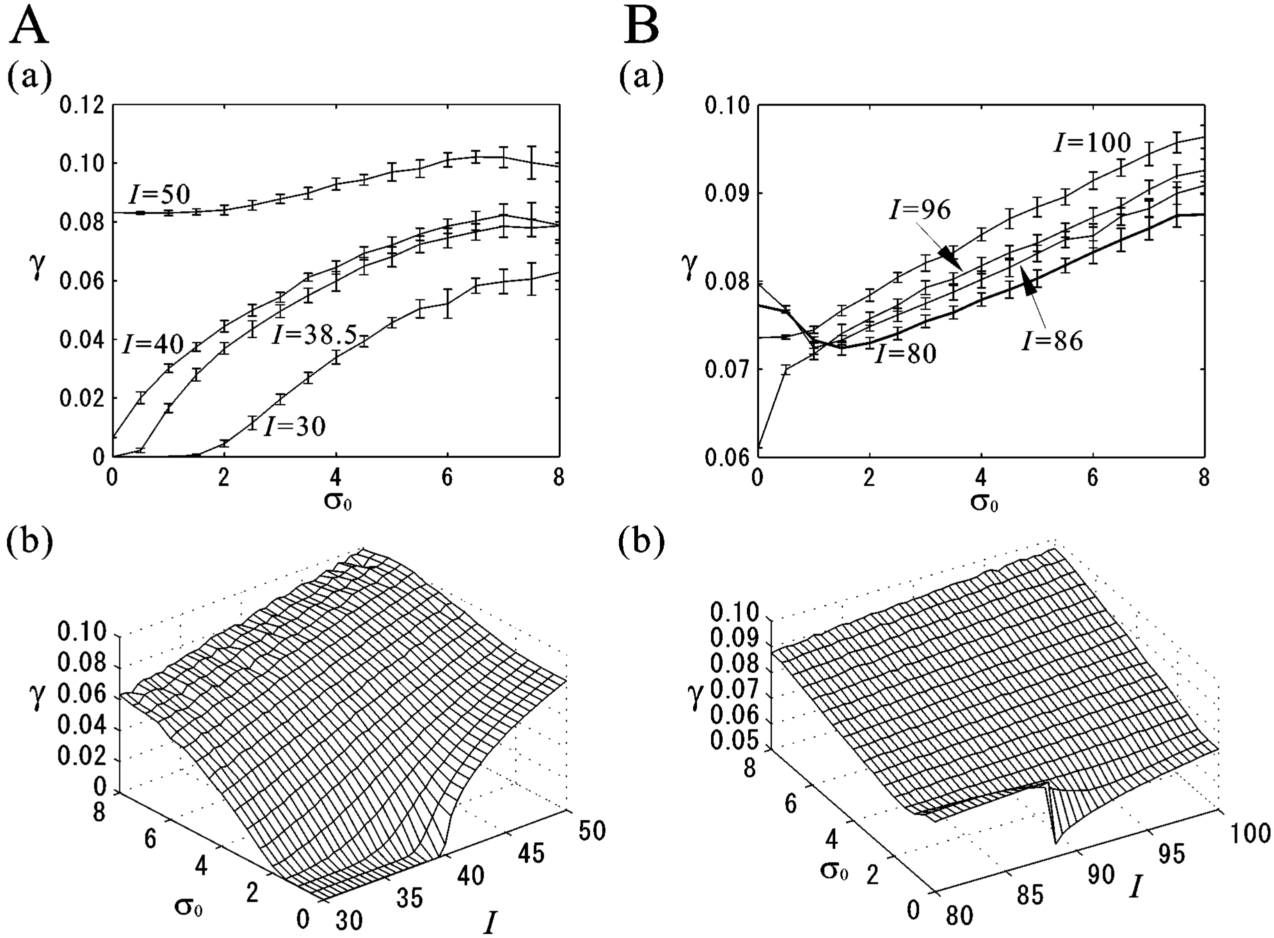

FIG. 9. Rotation numbers of the stochastic ML model. (A) The class I ML model. (a) Mean values and standard deviations of rotation numbers are shown against noise intensity for four different current values ($I=30$, 38.5, 40, and 50 μA/cm^2). The former two are in the excitable regime and the latter the oscillatory regime. The rotation numbers were calculated for 20 different noise realizations each time with the noise intensity $\sigma_0(=\sigma/C)$ ranging from 0 to 8 with a step of 0.5. (b) The rotation numbers γ on the parameter plane I-σ_0. The rotation numbers were calculated in the same way as part (a). (B) The class II ML model. (a) Mean values and standard deviations of rotation numbers against noise intensity for four different current values ($I=80$, 86, 96, and 100 μA/cm^2). The former two are in the excitable regime and the latter the oscillatory regime. (b) Average rotation numbers γ on the parameter plane $I-\sigma_0$.

tion number is close to zero in the class I ML model and close to a nonzero value (the imaginary part of the eigenvalues of the Jacobian matrix at the equilibrium) in the class II ML model. This is consistent with the value of the rotation number obtained in the deterministic regime. At large noise intensities, the situation becomes different, as noise-induced firing becomes frequent, and in fact, predominant as compared with subthreshold oscillations. In this case, the rotation number becomes an indicator of the rate of noise induced firings. This difference in the interpretations of the low and large noise limits of the rotation number are visible in Fig. 9. The transition between the two extremes is progressive and smooth but takes place within a narrow range of noise intensities. In this intermediate range of noise, the rotation number reflects the rates of both subthreshold and suprathreshold fluctuations.

These observations on the rotation number in the excitable regime are consistent with the quantitative changes of the stationary distribution reported in Sec. IV. The noise range where the rotation number is close to its deterministic value corresponds to the range where the stationary distribution takes on a Gaussian-type shape with a sharp peak centered on the equilibrium point. As the ring-like hump of the stationary distribution grows, the peak height decreases and the peak width increases, the rotation number moves away from the deterministic value towards the mean firing rate.

In the class I ML model, as one moves closer to the bifurcation separating the excitable and oscillating regimes, the range of noise where the rotation number remains close to zero (its deterministic value) before moving towards the firing rate, decreases [cf. curves labeled with $I=30$ and $I=38.5$ in panel (a) and a 3D representation in panel (b) in Fig. 9(A)]. This is consistent with the fact that noise induced firing is all the more frequent if the system is close to the bifurcation. At the bifurcation point, even weak noise induced fluctuations can lead to the generation of action potentials, as the system no longer possesses a firing threshold [a curve labeled with $I=40$ in panel (a) in Fig. 9(A)]. Hence, the rotation number, while starting at zero noise level, as in the excitable regime, moves along the firing rate as the noise is increased, as in the oscillating regime. In this sense, the noise-dependence of the rotation number at the bifurcation point is intermediate between the excitable and oscillating regimes.

The changes in the rotation number of the class II ML model, in the transition from excitable to oscillating regimes are more complex than those of the class I ML model. However, they are consistent with the changes in the stationary distribution. At low noise levels, the rotation number is close to some average of the two rotation numbers of the deterministic system associated to the stable equilibrium and the stable limit cycle. Roughly speaking, the contribution of each deterministic rotation number to the stochastic rotation number is weighted by the relative time the system spends near the corresponding attracting set (namely the stable equilibrium and the stable limit cycle). Thus, in the parameter and noise intensity ranges where the stationary distribution is either strongly and almost exclusively concentrated on the stable equilibrium point or on the limit cycle, the rotation number is close to one of the deterministic rotation numbers and reflects either the rate of subthreshold or suprathreshold oscillations. These two situations occur near either end of the bistable regime and mainly at weak noise intensities. Therefore, at low noise levels, there are no sharp changes in rotation number as one moves from either the excitable or the oscillating regimes into the bistable regime. The transition from rotation numbers close to the imaginary part of the eigenvalue of the Jacobian matrix at the stable equilibrium, to those close to the firing rate of the system on the stable limit cycle, occurs within the bistable regime, concurrently with the change in the shape of the stationary distribution, from those mainly centered on the equilibrium point to those mainly centered on the limit cycle.

The above considerations hold as long as the noise intensity is such that a distinction can be made between sub and suprathreshold noise induced fluctuations. At larger noise levels, beyond the feasible qualitative density change occurring in the bistable regime at which the peak on the equilibrium merges with the ring-like hump on the limit cycle no such distinction can be made. In this noise range, the rotation number reflects the overall rate of fluctuations in the system, with no particular distinction between sub and suprathreshold dynamics.

In summary, the changes in the rotation number of the models reflect those of the stationary distributions. In the class I regime no P-bifurcations take place, and the changes in the rotation number of the stochastic ML model as one moves from excitable to oscillating regimes follow the quantitative changes in the stationary distribution. In the class II regime, where there is the possibility that the system undergoes a P-bifurcation, the changes in the rotation number reflect this phenomenon. This major difference between the stochastic class I and class II membranes is illustrated by the two bottom panels in Fig. 9 that show 3D representations of the rotation number for the class I (left panel) and class II (right panel) models for values of the current I and noise intensity σ. The difference between the two forms at low noise levels, as one moves from excitable to oscillating regimes is clearly visible. While in both the transition is smooth at large noise levels, in the right panel, it is actually abrupt at low noise levels, giving the impression that it is discontinuous.

VII. DISCUSSION

This work presented a systematic analysis of a stochastic neuron model from the RDS theory standpoint. Studying the influence of noise on neuronal behavior has a long history.[35] However, those concerned with RDS analysis of neuronal response to noise like sample paths are scarce.[20–23] Our work presented the first RDS analysis of the ML membrane model. In this section, we discuss our results from the RDS and neuroscience standpoints.

The RDS analysis of the influence of random perturbations on deterministic bifurcations, and more generally that of stochastic D-bifurcations is an active field of investigation. As argued by Arnold,[16] this field has yet to reach its full development. Careful and systematic numerical explorations are instrumental in further developing this theory. This is all the more important in the case of systems perturbed by additive noise because for these it is not possible to readily apply the analytical methods of the RDS theory. In this respect, our study pursues others such as the one concerned with the Brusselator,[18] that have performed numerical analyses of randomly perturbed bifurcations.

The contribution of our numerical analysis to the RDS theory resides in the exploration of the influence of noise on two distinct bifurcation scenarios in the ML equations. The first scenario was that of the saddle node loop bifurcation separating the excitable and oscillating regimes in the class I ML model. We reported that noise destroys this bifurcation in the sense that the stochastic ML model possesses a unique stochastic equilibrium that attracts all trajectories. To our knowledge, this was the first analysis of the influence of additive noise on a saddle loop bifurcation. The second scenario was that of a double cycle bifurcation followed by a subcritical Hopf bifurcation. We had previously studied the influence of noise on this scenario in the FitzHugh–Nagumo (FHN) model.[22,23] Similarly to that study, we found here that low noise intensities destroy the bifurcation sequence. However, at larger noise intensities, the random dynamics of the class II ML and the FHN differ from one another. As reported in this work, the leading Lyapunov exponent of the ML model remains negative at all noise intensities. Conversely, the leading Lyapunov exponent of the FHN model is positive for some intermediate noise range indicating the presence of stochastic chaos. We attributed the occurrence of stochastic chaos in the FHN model to the existence of canard-like solutions. The influence of such solutions in the ML model is less marked thereby accounting for the difference between the two models.

Our work presented the RDS from a practical standpoint, as a means to investigate a biologically motivated problem. More precisely, we tackled the issue of neuronal reliability in response to noise-like realistic stimuli with the help of the RDS theory. While this problem has been fundamental for elucidating the neuronal code,[1] there have been few theoretical studies. This is where the contribution of this work lies.

As explained in Sec. II, experimental studies have led to the classification of membranes into class I and class II categories based upon their different response characteristics to various stimuli. Using the ML model, which is a widely used prototype for both classes, we examined the response of these to noise-like realistic stimuli. By examining the sign of the Lyapunov exponent, we have shown that modifying either the mean stimulus I or the intensity of the noise-like stimulus does not induce any dynamic stochastic bifurcation. From the standpoint of neuronal coding, this asymptotic stability of the stochastic attractor implies that to each noise-like input realization, there corresponds a unique asymptotic response. This means that if the ML model is initiated at a different state point and presented with the same input realization repeatedly, the same response will be evoked after a transient time. In this sense, the response evoked by such noise-like input is reliable.

These observations lead to our main conclusion which is that, as far as discharge time reliability is concerned, there is no difference between class I and class II ML models. Despite the differences in the deterministic regimes, in the responses to single and step currents, the ML model has the same asymptotic random dynamics in all regimes. Furthermore, this asymptotic behavior corresponds to reliable firing: the sequence of discharge times (after possibly some transient has elapsed) does not depend on the initial conditions. It corresponds to the stable stochastic equilibrium point.

The reliability notwithstanding, to different noise sample paths and to different parameter sets, there correspond different stochastic equilibria. It is in this latter aspect that the differences between the class I and class II ML models affect the response of the system to noise-like stimuli. Indeed, unlike deterministic equilibria, stochastic equilibria are themselves dynamical objects. Stochastic equilibria are stationary stochastic processes. The characteristics of these processes such as, say, their distribution can depend on model parameters. Our study revealed that as far as the stationary distribution and the rotation numbers are concerned, there are differences between the stochastic equilibrium of class I and class II ML models. In terms of neuronal coding, this result suggests that while both class I and class II membranes may be reliable, they may be sensitive to different stimulus characteristics and therefore use different "codes."

Based on spike characteristics and on response patterns during sustained applied currents, neural membranes can in general be classified into the two classes. The fact is well-known for a variety of neural preparations while little has been examined about those in the central nervous system like cortical neurons. Neocortical neurons are generally classified into three electrophysiological types: regular-spiking (RS), fast-spiking (FS), and intrinsically bursting.[36] Recently, Robinson reported that in the somatosensory cortex, the RS and FS types, respectively, show class I and II threshold behavior.[37] In addition, when applied currents are not enough to evoke a sustained spike generation, FS cells typically show subthreshold oscillations while RS cells do not. This implies that the characteristics investigated in this study could influence neural coding by modulating discharge time variability in actual neural systems such as neocortical circuits.

General considerations: In this study, we assumed that all transition pdfs of the stochastic ML model, whether in class I or class II regimes, stabilize at a unique stationary distribution. However, before the determination of P-bifurcations, we essentially needed to discuss the existence and the uniqueness of the stationary distribution for the stochastic ML model. As far as we know, there are no rigorous proofs of this fact and they are still open problems, while such an exceptional attempt was performed in Ref. 19. With respect to P-bifurcation, in addition, to search for shape changes of the stationary densities is actually a hard task to carry out without analytical solutions of the Fokker–Planck equation. Moreover, our methods in this study mainly resorted to the numerical calculations. The reason is that since the Gaussian white noise input acts as an additive perturbation to the ML model, it leaves no solution of the deterministic system invariant. As argued by Arnold *et al.*,[18] this makes it impossible to directly apply the analytical methods of the stochastic bifurcation theory.

ACKNOWLEDGMENTS

We thank Dr. Hugh P. C. Robinson (the University of Cambridge) for his valuable comments. One of the authors (T.T.) thanks Professor Shunsuke Sato and Professor Taishin Nomura (Osaka University) for their support. This work was in part supported by Grant-in-Aid for Scientific Research (B)(2)12480086 and Postdoctoral Fellowships for Research Abroad from the Japan Society for the Promotion of Science and a grant from the BBSRC.

APPENDIX

1. Parameters

Parameter values of the ML equations that we used are the same as those of the model described by Rinzel and Ermentrout.[24] The parameter values for the class I membrane model are: $V_K = -84$ mV, $V_L = -60$ mV, $V_{Ca} = 120$ mV, $C = 20\ \mu$F/cm^2, $g_L = 2.0\ \mu$S/cm^2, $g_{Ca} = 4.0\ \mu$S/cm^2, $g_K = 8\ \mu$S/cm^2, $V_1 = -1.2$ mV, $V_2 = 18$ mV, $V_3 = 12$ mV, $V_4 = 17.4$ mV, and $\phi = 0.067$. For the class II membrane model, they are the same described above except $V_3 = 2$ mV, $V_4 = 30$ mV, $g_{Ca} = 4.4\ \mu$S/cm^2, and $\phi = 0.04$.

2. Bifurcation diagrams

The bifurcation diagrams in Figs. 2 and 3 were constructed with AUTO (Ref. 7) as a component of XPPAUT software. More detailed information about the XPPAUT software can be found in Ref. 38.

3. Numerical integrals

In order to obtain an accurate approximation, the forward improved Euler or Heun method was used for the numerical integration of Eq. (3) with a time step of $\Delta t = 0.001$. The method gives a higher order discretization error than the simple Euler method explained in Ref. 39. Whenever much higher accuracy was needed we lowered the time step. However, we mainly used a fixed time unit of $\Delta t = 0.001$ through all of the numerical analysis presented here.

4. Stationary distributions

For the stationary distribution 200×140 points situated on a grid $\{(v,w)|-100\leq v\leq 100, 0\leq w\leq 1\}$ in the v-w phase plane were let iterate for the numerical calculation of Eq. (3) with a time step of $\Delta t=0.001$. The numerical calculation was carried out for 10^9 time units after discarding the first 10^4 time units. If a higher spatial resolution is needed, 600×420 points on the grid were used for the distribution. Points were subjected to stimuli with the same I_0 and σ. The stationary distribution emerged as the three-dimensional histograms of the final position of all points in the phase plane after normalization.

5. Lyapunov exponents and rotation numbers

The leading Lyapunov exponents of the system were estimated using the algorithm described in Ref. 39. They were calculated from an individual trajectory on the basis that the system under study is ergodic. The simulation run for a period long enough to insure convergence. Actually, the simulation time was 10^9 time units after a result of the first 10 000 time units was discarded. To estimate rotation numbers, we first calculated each angle of the successive two positions of the state point on the individual trajectory in the phase plane and accumulated the angles during the simulation time. The rotation number was finally obtained after dividing the angle by the simulation period. The mean and standard deviation out of 20 trials were used to neglect variation due to different realizations.

6. Pullbacks

For the pullbacks of panels in Fig. 8, a starting grid of 2500 points regularly positioned in the phase space was used as initial conditions. All trials evolved under the same input noise realization.

[1] J. A. Movshon, ''Reliability of neuronal responses,'' Neuron **27**, 412–414 (2000).
[2] C. Morris and H. Lecar, ''Voltage oscillations in the barnacle giant muscle fiber,'' Biophys. J. **35**, 193–213 (1981).
[3] K. Aihara and G. Matsumoto, ''Chaotic oscillations and bifurcation in squid giant axons,'' in *Chaos*, edited by A. V. Holden (Manchester University Press, Manchester, 1986), pp. 250–269.
[4] D. T. Kaplan, J. R. Clay, T. Manning, L. Glass, M. R. Guevara, and A. Shrier, ''Subthreshold dynamics in periodically stimulated squid giant axons,'' Phys. Rev. Lett. **76**, 4074–4077 (1996).
[5] D. H. Perkel, J. H. Schulman, T. H. Bullock, G. P. Moore, and J. P. Segundo, ''Pacemaker neurons: Effects of regularly spaced synaptic input,'' Science **145**, 61–63 (1964).
[6] N. Takahashi, Y. Hanyu, T. Musha, R. Kubo, and G. Matsumoto, ''Global bifurcation structure in periodically stimulated giant axons of squid,'' Physica D **43**, 318–334 (1990).
[7] E. Doedel and J. P. Kernevez, ''AUTO: Software for continuation and bifurcation problems in ordinary differential equations,'' Applied Mathematics Report, California Institute of Technology, 1986.
[8] K. Yoshino, T. Nomura, K. Pakdaman, and S. Sato, ''Synthetic analysis of periodically stimulated excitable and oscillatory membrane models,'' Phys. Rev. E **59**, 956–969 (1999).
[9] Z. F. Mainen and T. J. Sejnowski, ''Reliability of spike timing in neocortical neurons,'' Science **268**, 1503–1506 (1995).
[10] H. Bryant and J. P. Segundo, ''Spike initiation by transmembrane current: a white noise analysis,'' J. Physiol. (London) **260**, 279–314 (1976).
[11] J. Kröller, O. J. Grüsser, and L. R. Weiss, ''Observations on phase-locking within the response of primary muscle spindle afferents to pseudo-random stretch,'' Biol. Cybern. **59**, 49–54 (1988).
[12] J. D. Hunter, J. G. Milton, P. J. Thomas, and J. D. Cowan, ''Resonance effect for neural spike time reliability,'' J. Neurophysiol. **80**, 1427–1438 (1998).
[13] M. J. Berry, D. K. Warland, and M. Meister, ''The structure and precision of retinal spike trains,'' Proc. Natl. Acad. Sci. U.S.A. **94**, 5411–5416 (1997).
[14] J. Haag and A. Borst, ''Encoding of visual motion information and reliability in spiking and graded potential neurons,'' J. Neurosci. **17**, 4809–4819 (1997).
[15] P. Reinagel, ''Information theory in the brain,'' Curr. Biol. **10**, 542–544 (2000).
[16] L. Arnold, *Random Dynamical Systems* (Springer, Berlin, 1998).
[17] H. Crauel and F. Flandoli, ''Additive noise destroys a pitchfork bifurcation,'' J. Dynam. Differ. Eqs. **10**, 259–274 (1998).
[18] L. Arnold, G. Bleckert, and K. R. Schenk-Hoppé, ''The stochastic Brusselator: Parametric noise destroys Hopf bifurcation,'' in *Stochastic Dynamics*, edited by H. Crauel and M. Gundlach (Springer-Verlag, New York, 1999), pp. 71–90.
[19] L. Arnold and P. Imkeller, ''The Kramers oscillator revisited,'' in *Stochastic Processes in Physics, Chemistry, and Biology*, edited by A. Freund and T. Poschel (Springer-Verlag, Berlin, 2000), pp. 280–291.
[20] K. Pakdaman, ''The reliability of the stochastic active rotator,'' Neural Comput. **14**, 781–792 (2002).
[21] K. Pakdaman and S. Tanabe, ''Random dynamics of the Hodgkin–Huxley neuron model,'' Phys. Rev. E **64**, 050902(R) (2001).
[22] E. K. Kosmidis and K. Pakdaman, ''Analysis of reliability in the FitzHugh–Nagumo neuron model,'' J. Comput. Neurosci. **14**, 5–22 (2003).
[23] E. K. Kosmidis and K. Pakdaman, ''Stochastic chaos in a neural model,'' Int. J. Bif. Chaos (in press).
[24] J. Rinzel and G. B. Ermentrout, ''Analysis of neural excitability and oscillations,'' in *Methods in Neural Modeling*, edited by C. Koch and I. Segev (The MIT Press, Cambridge, 1989), pp. 135–171.
[25] A. L. Hodgkin and A. F. Huxley, ''A quantitative description of membrane current and its application to conduction and excitation in nerve,'' J. Physiol. (London) **463**, 391–407 (1952).
[26] A. L. Hodgkin, ''The local electric changes associated with repetitive action in a nonmedullated axon,'' J. Physiol. (London) **107**, 165–181 (1948).
[27] A. Arvanitaki, ''Recherches sur la résponse oscillatoire locale de l'axone géant isolé de sepia,'' Arch. Int. Physiol. **49**, 209–256 (1939).
[28] F. Brink, D. W. Bronk, and M. G. Larrabee, ''Chemical excitation of nerve,'' Ann. N.Y. Acad. Sci. **47**, 457–485 (1946).
[29] A. Lasota and M. C. Mackey, *Chaos, Fractals, and Noise* (Springer-Verlag, New York, 1998).
[30] Y. Liang and N. Sri Namachchivaya, ''P-bifurcations in the noisy Duffing–van der Pol equation,'' in *Stochastic Dynamics*, edited by H. Crauel and M. Gundlach (Springer-Verlag, New York, 1999), pp. 49–70.
[31] L. Arnold, ''The unfolding of dynamics in stochastic analysis,'' Matemática Aplicada e Computacional **16**, 3–25 (1997).
[32] H. Kunita, *Stochastic Flows and Stochastic Differential Equations* (Cambridge University Press, Cambridge, 1990).
[33] V. I. Oseledets, ''A multiplicative ergodic theorem. Lyapunov characteristic numbers for dynamical systems,'' Trans. Moscow Math. Soc. **19**, 197–231 (1968).
[34] P. Ashwin and G. Ochs, ''Convergence to local random attractors,'' Dynamical Systems **18**, 139–158 (2003).
[35] J. P. Segundo, J.-F. Vibert, K. Pakdaman, M. Stiber, and O. Diez-Martínez, ''Noise and the neurosciences: A long history with a recent revival (and some theory),'' in *Origins: Brain and Self Organization*, edited by K. Pribram (Lawrence Erlbaum Associates, Hillsdale, 1994), pp. 299–331.
[36] M. J. Gutnick and W. E. Grill, ''The cortical neuron as an electrophysiological unit,'' in *The Cortical Neurons*, edited by M. J. Gutnick and I. Mody (Oxford University Press, New York, 1995), pp. 33–51.
[37] H. P. C. Robinson, ''The biophysical basis of firing variability in cortical neurons,'' in *Computational Neuroscience: A Comprehensive Approach*, edited by J. F. Feng (CRC Press, London, 2004) (in press).
[38] B. Ermentrout, *Simulating, Analyzing, and Animating Dynamical Systems: A Guide to XPPAUT for Researchers and Students* (Society for Industrial and Applied Mathematics, Philadelphia, 2002).
[39] P. E. Kloeden and E. Platen, *Numerical Solution of Stochastic Differential Equations* (Springer-Verlag, Berlin, 1999).